Gold-based hybrid nanomaterials for biosensing and molecular diagnostic applications

Jung Eun Kim, Ji Hye Choi, Marion Colas, Dong Ha Kim, Hyukjin Lee

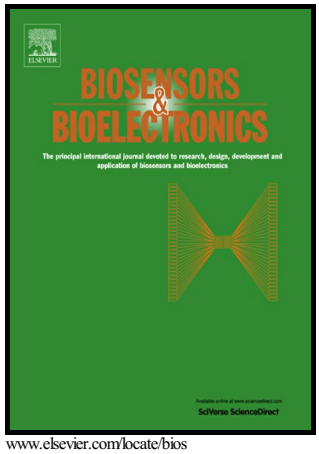

www.elsevier.com/locate/bios

PII: S0956-5663(16)30123-3
DOI: http://dx.doi.org/10.1016/j.bios.2016.02.015
Reference: BIOS8447

To appear in: *Biosensors and Bioelectronic*

Received date: 1 December 2015
Revised date: 23 January 2016
Accepted date: 6 February 2016

Cite this article as: Jung Eun Kim, Ji Hye Choi, Marion Colas, Dong Ha Kir and Hyukjin Lee, Gold-based hybrid nanomaterials for biosensing and molecula diagnostic applications, *Biosensors and Bioelectronic* http://dx.doi.org/10.1016/j.bios.2016.02.015

Gold-based hybrid nanomaterials for biosensing and molecular diagnostic applications

Jung Eun Kim†[a], Ji Hye Choi†[b], Marion Colas†[a,c], Dong Ha Kim*[b], and Hyukjin Lee*[a]

[a] College of Pharmacy, Graduate School of Pharmaceutical Sciences, Ewha Womans University, Seoul 03760, South Korea

[b] Department of Chemistry and Nano Science, Ewha Womans University, Seoul 03760, South Korea

[c] Faculté de Pharmacie de Paris, Université Paris Descartes, Paris, France

† These authors contributed equally to this work.

Correspondence to

Dong Ha Kim: dhkim@ewha.ac.kr

Hyukjin Lee: hyukjin@ewha.ac.kr

Abstract

The properties of gold nanomaterials are particularly of interest to many researchers, since they show unique physiochemical properties such as optical adsorption of specific wavelength of light, high electrical conductance with rich surface electrons, and facile surface modification with sulfhydryl groups. These properties have facilitated the use of gold nanomaterials in the development of various hybrid systems for biosensors and molecular diagnostics. Combined with various synthetic materials such as fluorescence dyes, polymers, oligonucleotides, graphene oxides (GO), and quantum dots (QDs), the gold-based hybrid nanomaterials offer multi-functionalities in molecular detection with high specificity and sensitivity. These two aspects result in the increase of detection speed as well as the lower detection limits, having shown that this diagnosis method is more effective than other conventional ones. In this review, we have highlighted various examples of nanomaterials for biosensing and molecular diagnostics. The gold-based hybrid systems are categorized by three distinct detection approaches, in which include 1) optical, such as surface plasmon resonance (SPR), RAMAN, and surface-enhanced Raman scattering (SERS), 2) fluorescence, such as förster resonance energy transfer (FRET) and nanomaterial surface energy transfer (NSET), and 3) electrochemical, such as potentiometic, amperometric, and conductometric. Each example provides the detailed mechanism of molecular detection as well as the supporting experimental result with the limit of detection (LOD). Lastly, future perspective on novel development of gold-based hybrid nanomaterials is discussed as well as their challenges.

Key words: Gold nanomaterials, Biosensor, Molecular Diagnostic, Surface Plasmon Resonance, Hybrid Materials

Contents

1. Introduction

Biosensors can detect an analyte using a biological probe, coupled to a detection device. When applied to the molecular diagnostics field, the analyte is a biomarker whose detection in a biological sample is determinant for a specific condition to provide the disease diagnosis, evaluation of the disease stage, and monitoring of its progresses and treatments. The various natures of biomarkers necessitate a variety of biosensors adapted to each marker, which is more facile, fast, sensitive and highly specific.

Gold nanomaterials have been widely used in the past decade due to their unique optical, electrical, and chemical properties over the conventional inorganic nanomaterials such as silica (SiO_2) (Song et al. 2009), quantum dots (QDs) (Yue et al. 2013), and lanthanide nanoprobes (Zheng et al. 2015b). The optical properties of gold nanomaterials strongly depend on the shape of materials such as nanostars (NSts) (Nehl et al. 2006), spherical nanoparticles (NPs) (Hu et al. 2015), nanorods (NRs) (Huang et al. 2007), nanopyramids (Wang et al. 2012), or nanojavelins (Chateau et al. 2015). Since the surface plasmon resonance (SPR) by the specific oscillation of electron cloud on the surface of gold nanomaterials depends on the length, cross section of materials, and surrounding medium, the precise control of these properties provides exceptional multi-functionalities for applications in biosensing and molecular diagnostics.

Various hybrid materials of gold nanomaterials combined with other components have been developed to expand their uses. Facile surface modification of gold materials has been reported with proteins (Chen et al. 2015), polymers (Zhang et al. 2015a), graphene oxide (GO) sheets, fluorescent dyes (Zhang et al. 2015b), oligonucleotides (Wijaya et al. 2009), and other inorganic materials by the thiol-gold reaction or non-specific charge interaction. Combined with the unique optical properties of gold nanomaterials that adsorb a certain wavelength of the light, these hybrid nanomaterials have been extensively used for various applications in light responsive drug delivery (Wijaya et al. 2009) and molecular diagnostic systems (Chen et al. 2015; Hu et al. 2015; Kim et al. 2010; Qin et al. 2015a). In addition to the optical properties, gold nanomaterials have

excellent electrical and chemical properties. Due to the high conductivity from rich electrons and large surface area, gold nanomaterials can be used as conductive tags for the electrical sensors for identifying different target biomolecules. The changes in the ohmic response of the circuit or the currents triggered from the faradaic process near the surface of electrodes can explain the appearance of these characteristics (Wittenberg and Haynes 2009).

In this review, we highlight the state-of-the-art development of gold-based hybrid nanomaterials for biosensing and molecular diagnostics. Depending on the detection methods, three distinct approaches have been categorized: optical (SPR, Raman, SERS), fluorescence (FRET, NSET), and electrochemical (potentiometic, amperometric, conductometric). These biosensors are detailed in **Table 1**, along with their characteristics, uniqueness, and detection methods. This review provides a general overview of gold-based hybrid nanomaterials for readers from a broader field, while each material example is extensively reviewed and discussed in detail. Lastly, the future prospects and challenges in the development of gold-based hybrid biosensor are provided.

2. Au-based Hybrid Materials used for biosensors

2.1. Optical detection by Au-based Hybrid Materials

2.1.1. SPR and SERS of Au and Au-based Hybrid Materials

Although SPR depends on the length, cross-section and environment (surrounding medium) of the gold nanomaterial (Mühlschlegel et al. 2005; Ono et al. 2005; Sönnichsen and Alivisatos 2005), the properties of a single NP were explored (Huang et al. 2007), in particular, the relationship between the incident light and the SPR induced on an isolated single NR (by simple polarization contrast microscopy). After preparation, NRs had an average diameter of 125 nm, for a 1.45 μm length, which led to an aspect ratio of 12. This single NR was located far from other NPs in order to avoid interference, and the resulting far-field image showed several dark fringes on the gold NR (AuNR), which exemplified occurrences of multipolar SPR modes (Félidj et al. 2006; Seidel et al. 2004).

An equation was then established, after calculating the SPR modes wave vectors, in order to enlighten the relationship between the incident light and the induced SPR modes.

The SPR band varies according to parameters such as the composition, shape, or size of an NP. In consequence, these characteristics can be tuned to fit certain purposes (Kim et al. 2011). In one particular case, gold nanobipyramids were synthesized with the precise control of the shape, size and, truncation of the particle in order to control the longitudinal SPR band (between 600 and 2000 nm, as opposed to simple spherical gold NP (AuNP) with a small range of 500-600 nm) (Chateau et al. 2015). As the surfactant defines the particle morphology, instead of using classic cetyltrimethylammonium bromide (CTAB), polycrystalline seeds were grown with a mix of both CTAB and cetyltrimethylammonium chloride (CTAC). The result was the acquisition of elongated bipyramids with a length in the range of 130 to 300 nm, and an aspect ratio from 6 to 14. Nanojavelins exhibited resonance toward the IR wavelength, in the 1,400-1,800 nm range.

To further investigate the complexity of gold nanostructures, Nehl *et al.* synthesized star-shaped AuNPs incorporating polarization-dependent scattering with multiple spectral peaks and a strong dielectric sensitivity (Nehl et al. 2006). **Fig. 1A and 1B** show the morphology of star-shaped AuNPs with one to 6 tips. The surfactant, CTAB, was replaced by a 10 nm diameter gold colloid during the preparation of the AuNRs to obtain 100 nm star-shaped AuNPs. The extinction spectra (**Fig. 1**) suggest the peaks in both visible and broad near infrared (NIR) regions. The first peak (773 nm) is attributed to longitudinal plasmon resonance due to the elongated tip structure of the particle, and the second (586 nm) to the transverse plasmon resonance. The optical properties of a single NS were also investigated; however, there were just few peaks found in the spectrum, indicating multiple peaks at a same wavelength or peaks outside the detection. These stars also have a strong dielectric sensitivity and sharp NIR resonances, so they would make good substrates for localized surface plasmon resonance (LSPR) sensors.

Another challenge in producing AuNPs with branched morphology was the control of the number of arms and their length. This was achieved by the synthesis of gold nano-hexapods with seeded growth in the presence of single-crystal Au octahedral (Kim et al. 2011). The LSPR spectrum revealed peaks shifting from the visible to the near infrared

region (555 nm to 880 nm) depending on the arm length. It has been shown that the length of arm could be controlled by varying the amount of $HAuCl_4$ (increasing the concentration increased the arm length), or the temperature (increasing the reaction temperature decreased the arm length), or both. As opposed to the seed growth on the arms of octahedral, the core did not change in size relative to the arms. Regarding the optical properties, gold nano-hexapods displayed two LSPR peaks: dipolar resonances at the tips or the central core. Increasing the amount of $HAuCl_4$ caused a red-shift of the LSPR peak as the arm length increased as well, and above a certain condition (~10 µl), a blue-shift was observed due to a reduction of the aspect ratio. There also was a linear relationship between the LSPR peak position and the reaction temperature (a blue-shift with increasing temperature).

An AuNP itself has its own optical properties, and as an ensemble, or hybridized with another molecule, these characteristics can also vary and so be tuned (Cheng et al. 2003; Cheng et al. 2002; Liu et al. 2014; Ng et al. 2012). For example, by hybridizing specific polymers to AuNPs, oligomers reversibly assemble themselves and the interparticle spacing can be precisely controlled, as well as their resulting spectroscopic properties (Zhang et al. 2015a). **Fig. 2A** shows the scheme of the nanomaterial structures. These AuNPs (diameter 25 nm) were decorated with both poly(ethylene glycol) (PEG) and 2,2'-Dithiobis[1-(2-bromo-2-methyl-pro-pionyloxy)] Ethane (DTBE) through Au-S bond interaction. Subsequently, the surface was polymerized with photo responsive spiropyran-containing methacrylate monomer (PSPMA). The use of this polymer facilitated the reversible self-assembly into aggregates with a controlled number of NPs by light irradiation (Cheng et al. 2011; Samanta and Locklin 2008; Schöller et al. 2014; Song et al. 2011). As shown in **Fig. 2B**, spiropyran units are thereby transformed into zwitterionic mecyanine isomer upon irradiation by UV light, leading to strong electrostatic interaction and hence self-assembly of oligomers. **Fig. 2C** shows the UV-vis absorption spectrum which was used to investigate the photo responsive behaviors of Au-PEG/PSPMA. When small amounts of water (volume fraction of 10 %) were added to the AuNP solution, the spectrum showed a slight increase in the range of 640-800 nm, indicating the formation of some aggregates. The addition of H_2O triggered shrinkage of PSPMA material which reduced the distance between adjacent Au-PEG/PSPMA NPs.

The same result was obtained by irradiating the solution of AuNPs by UV light for 4h, and the color changed from pink to purple. When exposed to visible light, the color change was reverted, confirming the reversible aspect of the aggregation process. Measurement of the Raman bands revealed that the signals returned to their original values when the AuNPs were disassembled. An optical image of the color change is presented in **Fig. 2D**.

With its very own optical properties, GO has also been studied as an additional functionalizing agent when coupled to AuNPs. For example, GO nanosheets (nGO) were wrapped around gold NSts (AuNSts) to enhance the SERS signal (Jalani and Cerruti 2015). AuNSts were used as plasmonic enhancers, and nGO was used both as Raman reporter and SERS enhancer (Fan et al. 2014; Xu et al. 2013). The NPs were obtained by the self-assembly of negatively charged nGO sheets after modification of the AuNP surface by adding positively charged cysteamine groups (Zhu et al. 2010). nGO wrapping increased the SERS effect and prevented the desorption of eventual Raman dyes in physiological conditions, which could enhance the stability of the dye-based SERS probes. Moreover, as nGO contains residual functional groups (carboxyls, epoxides, hydroxyls), specific targeting could be achieved by conjugating biological compounds. Following a similar pattern, another study explored the enhancement of the Raman signal of graphene as it coats the surface of gold nanopyramids, resulting in a cooperative plasmonic resonance (Wang et al. 2012). A new D-band appeared in the Raman spectrum, but not when graphene was coated onto a flat gold surface, and was therefore attributed to sharp graphene folds near the pyramids tips; the enhancement factor was up to 10^7 times.

2.1.2. Gold-based hybrid materials for optical biosensing applications

When hybridized with specific antibodies, AuNPs can be used as efficient biosensors. In this example, a multi-arrayed LSPR chip was developed for the detection of multiple cytokine biomarkers requiring very small quantities of serum samples (Chen et al. 2015). The cytokines used in this device can predict the development of organ damage and bacterial infections (Ray et al. 2005; Wang et al. 1999). As shown in **Fig. 3A**, this chip

contained a microfluidic pattern and antibodies were conjugated with AuNRs, allowing quantitative cytokine measurement (range: 10-10000 pg/mL for 1 µL of serum) in 40 minutes. The AuNRs were dispersed into the device via electrostatic interactions between the AuNRs and the glass surface and the average particle-to-particle distance remained greater than 200 nm (~1 particles per 2.56 μm^2), thereby avoiding electromagnetic coupling between NPs (**Fig. 3B**). The detection method used dark-field imaging, and scanning the scattering of light intensity across the LSPR biosensing spots. The use of NPs showed enhanced sensitivity, as the analyte surface binding results in a red-shift in the resonant Rayleigh scattering spectrum (**Fig. 3C**) (Anker et al. 2008; Cao et al. 2014; Haes et al. 2004). Moreover, compared to the conventional sandwich immunoassays, a very short incubation time (1-fold) was required due to a rapid analyte binding. The assay also exhibited negligible cross-reactivity and a limit of detection (LOD) surpassing multiplex ELISA assay (Ikami et al. 2010).

Photoacoustic (PA) imaging is an active area of research if the diagnostics field, as it incorporates high spatial resolution, deep penetration depth, non-ionizing radiation, non-invasive imaging techniques and optically functionalized techniques (Wang and Hu 2012; Wang et al. 2003). Its signal amplitude can be increased by the NPs and AuNRs encapsulated within a reduced GO (r-GO) shell (Moon et al. 2015). These NPs present a characteristic peak at 230 nm in the UV spectrum, due to the presence of r-GO, a red-shifted absorption peak (from 230 to 270 nm) and a longitudinal plasmonic band (750 nm), specific to the AuNRs. r-GO AuNRs exhibited stronger PA signal intensities than did AuNR or GO AuNR, which would allow a lower input laser energy to use this technique for imaging applications with minimal damage to normal tissues in animal model studies (Kim et al. 2009). Moreover, by evaluating the PA signal amplitudes, rGO AuNRs provided a stronger response at a frequency enabling the visualization of target organs located deep in the body. The reduction of GO sheets was the key to enhancing the PA signals.

Another study within the biosensing field is the development of a double-enhanced lateral flow strip biosensor for the detection of protein biomarkers (Qin et al. 2015a). AuNPs were used to amplify the signal due to their surface plasmon properties

and high chemical stability (Li et al. 2010). Horseradish peroxidase (HRP) was used as an enhancer due to its catalytic efficiency, specificity, and enzyme activity (Reddaiah and Madhusudana Reddy 2014). The device was tested using CEA (carcino-embryonic antigen), MUC1 and thrombin recognition. A sample solution containing CEA and HO-AuNP-DNA (hairpin oligonucleotide and DNA attached onto the AuNP) was loaded in the pad, the complexes migrated through the device and the first red band was generated by AuNP accumulation as activated biotins were captured by the preimmobilized streptavidin (SA). The excess continued to migrate and met with SA-cHO (complementary to the hairpin loop), causing their hybridization and another accumulation of AuNP, causing another red band. They established a linear relationship between the peak area and the CEA concentration in the range of 5 fg/mL-20 ng/mL with a LOD of 2.9 ng/ml.

Nucleotide sequences (RNA or DNA) are also used as biomarkers, as in the example of cancer, where an abnormal expression of microRNA (miRNA) occurs both in the precancerous stage and in malignant cells (Bottoni et al. 2005). To detect this type of marker, a biosensor based on individual AuNP modified with a single-strand DNA (ssDNA) was utilized (Hu et al. 2015). This DNA strand can form a hairpin once attached onto the metal surface. The hairpin breaks when the sample is added, after which the target oligonucleotide can bind to its complementary sequence at the 5' end of the ssDNA. This phenomenon can be monitored by surface plasmon resonance scattering (SPRS) spectroscopy as the specific binding results in a red-shift in the SPRS spectrum. This shift was proportional to the target concentration for the range from 10 nM to 20 μM and LOD was evaluated at 3 nM. mi-RNA21 was used as it is overexpressed in many types of cancers (Asangani et al. 2007; Chan et al. 2005; Dillhoff et al. 2008; Meng et al. 2007; Takamizawa et al. 2004). As compared with a random RNA sequence, the shift of the target miRNA which can be the complementary miRNA sequence or a single-mismatch RNA sequence was distinct from the others, demonstrating the high specificity of the sensor.

Biosensing using the surface enhanced Raman scattering (SERS) properties of gold nanomaterials is widely studied, mostly due to its excellent molecular fingerprinting and

the anti-interference ability (Banholzer et al. 2008; Haynes and Van Duyne 2003; Li et al. 2015; Mayer and Hafner 2011; Zhao et al. 2008). A noticeable device permitted the detection of metallic ions (silver and mercury) in human saliva (Zheng et al. 2015a). 2015). The biosensor coupled a sandwich-based SERS probe (Li et al. 2012) to a gold nanohole array pattern. Sandwiches include a plasmonic gold core (in this case, a nanostar) surrounded by a thin silica-shell, and the Raman reporter molecules (malachite green isothiocyanate – MGITC) in between. The nanomaterials were then functionalized with ssDNA which hybridized in the presence of the ion due to T-T or C-C mismatch. SERS peak spectra were directly correlated to the ion concentration (proportional to the logarithmic concentration of silver (I) ion) until saturation. The same phenomenon was observed regarding mercury (II) and the LOD evaluated at 2.3 pM. Another device based on the SERS properties of gold nanoparticles, was developed and tested for biosensing of DNA strands and mercury ions (Yi et al. 2013). This method differs from the previous cited because it is based on the use of unmodified gold nanoparticles, simplifying the preparation process. Also, the improvement compared to colorimetric methods is an increase of the signal-to-background ratio. Regarding DNA detection, the target single stranded DNA hybridizes to the probe DNA, and after addition of the AuNPs (30 nm diameter), the Raman reporter molecule (crystal violet) and NaCl (35 mM), AuNPs aggregate leading to a stronger SERS signal. The LOD is 10 nM regarding DNA biosensing. The mechanism is similar to detect mercury ions, as in the presence of Hg^{2+}, mercury-mediated base pairs are formed thanks to thymine residues, transforming the probe into a hairpin structure. This structure then behaves like a double stranded hybrid, aggregating AuNPs and amplifying the SERS signal with a LOD of 0.2 µM.

Another method allows label-free scanometric detection of DNA by utilizing the electrostatic interactions between Au and DNA hybridized with neutral peptide nucleic acid (PNA) (Fabris et al. 2007; Kodama et al. 2009; Ongaro et al. 2004; Zhang et al. 2009). The assay was conducted for the detection of H5-type bird influenza virus, and allowed the naked-eye detection of the probe (Kim et al. 2010). The structure of this device is illustrated in **Fig. 4A**. The neutral PNA probes and their blocking materials were immobilized on the slide glass, then the target DNA was hybridized with PNA to give a negatively charged surface. When positively charged AuNPs were introduced, they

selectively bound to the PNA/DNA assembly to give a complex that could be observed by the naked eye or an optical scanner. As the smallest AuNPs had better accessibility to the space between target DNAs (Fang et al. 2008), because 1.4 nm AuNPs exhibited the strongest signal intensity and background, the optimal AuNP diameter was evaluated at 4 nm for an optimum metal enhancement process. **Fig. 4B** shows the optical images of processing experiments. Grayscale values were proportionally increased depending on the concentration of target DNA. The range of target DNA detection extended from 10 pM-100 nM, and exhibited comparable sensitivity to the fluorescence detection method (**Fig. 4C**).

Functionalized AuNPs were also tested for the detection of Shiga-toxin producing Escherichia coli (STEC) (Quintela et al. 2015). This study has developed a method for simultaneous detection of STEC strains, producing either stx1, or stx2, or both, by an optical biosensing method with oligonucleotide-functionalized AuNPs and DNA sandwich hybridization. **Fig. 5A and 5B** illustrate the mechanism of detection method in this sensor. AuNPs sized 13 nm absorbed green light at ~520 nm so solutions of AuNPs exhibited a red color, which remained unchanged after hybridization with the target genes (complexes stabilized AuNPs even in increased salt concentrations), whereas the solution containing AuNP-probes and non-complementary sequences displayed a color change from red to purplish-blue (aggregation under high salt concentrations). The UV-Vis absorbance spectrum in **Fig. 5E** reveals a broadening of the peaks toward longer wavelengths for the non-target because of particle aggregation, compared with the target strains which showed no change in the peak position but merely a reduced intensity due to dilution. The LOD was 1 log CFU/mL (even in food samples), and the method was compared with PCR and gel electrophoresis, which showed similar results.

Not only can AuNPs be used as biosensors for proteins or DNA sequences, they can also be used to detect small molecules. The main difference, and challenge, of detecting small molecules using LSPR is the fact that the binding of these substances induces a smaller change in the refractive index than the larger biomolecules do. An example of small molecule detection is a reusable biosensor for ochratoxin A (OTA) (Park et al. 2014), based on LSPR detection of the target binding to an aptamer immobilized on the

surface of AuNRs. This binding leads to the formation of a stable G-quadruplex structure (Chiu and Huang 2009; Yang et al. 2011) which induced a red-shift of the LSPR peak, and a linear relationship has been established between the LSPR peak and the OTA concentration in the range from 0.1 nM-10 μM. Moreover, the utilization of an aptamer enableds the device to be regenerated after use by heating in methanol at 70°C.

2.2. Fluorescence detection by Au-based Hybrid Materials

Numerous biosensing devices have been developed using AuNPs' unique optical properties and their ability to detect various biomarkers of diverse natures by a change in their spectrum or color. However, gold nanomaterials can also quench a wide range of fluorescence, which has led to the design of different types of biosensors. Measuring of the fluorescence signal is a common assay for the detection and identification of target molecules. To emit the fluorescence signal, organic dyes and QDs are often utilized. Generally, a wide range of organic dyes have been developed as fluorescent labels, but they have lower absorption coefficients and weaker fluorescence signals than QDs. In addition, organic dyes are prone to photo bleaching, which inhibits their use in long-term tracking. Therefore, the development of novel fluorescent probes with strong signal and photo stability remains highly desirable.

Two fluorescent detection methods are most commonly used: förster resonance energy transfer (FRET) and nanomaterial surface energy transfer (NSET). First, FRET is a spectroscopic technique in which the energy is transferred from one dye molecule (donor) to the other dye molecule (acceptor) *via* a dipole-dipole interaction. This energy transfer facilitates the observation of both the decrease in the donor's fluorescence emission and the increase in the acceptor's fluorescence emission intensities (Chen et al. 2012). FRET has been widely applied for disease detection and diagnosis because of its characteristics of high sensitivity, and rapid and easy quantitative evaluation with real time analysis (Liu et al. 2011; Tao et al. 2014). FRET is a distance-dependent technique and it can be useful for measuring molecular interactions in the small distance between 1

and 10 nm (dos Remedios and Moens 1995; Huang et al. 2012; Sekar and Periasamy 2003). The detection length of FRET is limited by the dipole-dipole interaction in nature, which induces the electronic inter band transition in the energy acceptor (Tao et al. 2014). This range is usually enough to observe very short dynamic interactions between proteins, nucleic acids, and cell membranes (Lilley and Wilson 2000; Parkhurst et al. 2002; Selvin 2000). However, most of other biomolecular processes have longer interaction distances and their dynamics and interactions are difficult to observe using FRET (Samanta et al. 2014). In addition, problems of low fluorescence signal and photo bleaching remain due to the inherent nature of organic dyes. To resolve these disadvantages, researchers have utilized other materials, such as AuNPs and QDs, to develop a technique called NSET. NSET is also generated by a dipole-dipole interaction in nature. In NSET, an energy transfer between donor and acceptor is similar to FRET. However, NSET is different from FRET because the NP, which is an acceptor, has a large surface area and an isotropic distribution of dipole vectors, which enable it to accept energy from the donor. Compared to FRET, the efficient quenching distance of NSET is estimated to reach more than 50 nm.

2.2.1. Gold-based hybrid materials for fluorescence-based biosensing applications

AuNPs show good biological stability (Borriello et al. 2009; Ghosh and Chattopadhyay 2013; Hu et al. 2009) and are great FRET-based quenchers, since they have large extinction coefficients and broad energy absorption bandwidth in the visible range (Chen et al. 2012). Therefore, AuNPs have attracted significant research interest in the applications of single-particle tracking (SPT) (Xu et al. 2007), cell imaging (He et al. 2008; Jiang et al. 2008; Wang et al. 2010), bioanalytes (Bi et al. 2009; Huang et al. 2013; Storhoff et al. 2004; Taton et al. 2000) and NSET (Oh et al. 2005). **Fig. 6** illustrates a good example of hybrid AuNPs for the fluorescence detection of analytes. As a quenched state, the AuNPs are physically complexed with charge complementary fluorescent dyes in close proximity (**Fig. 6A**) (Boisselier and Astruc 2009; Fan et al. 2003; Tan et al. 2015; You et al. 2007). In the presence of target proteins, the subsequent binding of protein analytes can substitute the fluorescence dyes, leading to the recovery of

fluorescence signal. Depending on the interaction and replacement of fluorescence dyes on the surface of AuNPs, separate fluorescence recovery signals and their response patterns can be obtained to distinguish the target proteins (**Fig. 6B**). This protein-sensing method by simple replacement of fluorophores offers impressive applicability for disease diagnosis; however, problems of low sensitivity and device specificity remain due to the diversity and complexity of proteinanalytes (You et al. 2007).

To overcome the above problems, You *et al.* have developed an alternative protein detection method. They used six fabricated cationic AuNPs were used for protein sensors and a highly fluorescent polymerpoly(*p*-phenyleneethynylene) (PPE) derivative (Bunz 2005; Swager and Zheng 2005), anionic carboxylate-substituted PPE (PPE-CO_2) (Kim et al. 2005), which is a fluorescence indicator. Various proteins with different molecular weights and isoelectric points (pI) were used as the target analytes. They added 5 μM of proteins into PPE-CO_2 (100 nM) and allowed the disruption of NP-PPE-CO_2 by proteins. Bovine serum albumin (BSA), β-galactosidase (β-Gal), acid phosphatase (PhosA), and alkaline phosphatase (PhosB) induced different levels of increasing fluorescence, while cytochrome *c* (CC) showed a decrease of fluorescence. In addition, Lipase and Subtilisin A (SubA) exhibited a small fluorescent change (**Fig. 7A**). However, the fluorescence response patterns of 5 μM proteins differed from the fluorescence response patterns with identical absorbance at 280 nm (**Fig. 7C**). You *et al.* also tried to calculate the canonical scores by linear discriminant analysis (LDA) (**Fig. 7B and 7D**), which exactly differentiates the protein pattern. NP-PPE assembly arrays against 5 μM proteins (**Fig. 7B**) or proteins with the identical absorption at 280 nm (**Fig. 7D**). The canonical score was calculated by LDA.

Another interesting example is measuring the intracellular reactive oxygen species (ROS) generation within live cells. 2', 7'-Dichlorodihydrofluorescein (DCFH) and 2-[6-(4'-amino)phenoxy-3*H*-xanthen-3-on-9-yl] benzoic acid (AFP) are commercialized fluorescent probes that are widely used for the detection of ROS in the cell. However, these fluorescent probes suffer the disadvantages of low photo stability and signal to noise ratio (Setsukinai et al. 2003). To resolve the problems, AuNP-based fluorescent probes have been developed by Lee and coworkers (Lee et al. 2009). Hyaluronic acid

(HA) is a natural polysaccharide found mostly abundantly in mammalian extracellular matrix (ECM) and used for selective detection of ROS. Excessive ROS generation can cause rapid degradation of high molecular weight HA in nature. To mimic this phenomenon, Lee *et al*. have prepared fluorescence probes composed of fluorescein-labeled HA and AuNPs. First, they used dopamine end-functionalized HA, which was labeled with multiple fluorescein molecules (**Fig. 8A**). The catechol group in dopamine showed very strong binding affinity toward the surface of the AuNPs and successful end immobilization of fluorescence labeled HA was performed. Due to the NSET between the fluorescence labeled HA and the AuNPs, the developed probes showed strong fluorescence quenching and minimally emitted the fluorescence signal. When ROS was added into the solution (AuNP-HA), the backbones of HA were degraded by ROS and the fluorescence molecule was released from the surface of the AuNPs, leading to the fluorescence turn-on. The developed probes showed enhanced ROS sensitivity (under 5 µM) as compared to the commercial probes toward superoxide anions ($^{\cdot}O_2^-$) and hydroxyl radicals ($^{\cdot}OH$) in the concentration rage of 1-100 µM with ROS detection limits (20 µM of $^{\cdot}O_2^-$ and 5 µM of $^{\cdot}OH$). A high signal to noise ratio was obtained using AuNP-based fluorescence probes. Lee *et al*. also used confocal laser-scanning microscopy (CLSM), which provided images of the intracellular ROS generation in macrophage cells (**Fig. 8C**). They found that AuNPs-HA are capable of live monitoring of intracellular ROS generation when treated with 1 µg/mL of LPS. Time dependent fluorescence (green) signal indicated the ROS-induced cleavage of AuNP-HA conjugates over the incubation time and Hoechst 33628 (blue) was used for staining the nucleus of cells.

For other small analyte detection such as H_2O_2, glucose, and uric acid, Huang *et al*. prepared AuNPs conjugated with horseradish peroxidase (HRP) and BSA (Huang et al. 2012). The probe consisted of the fluorescence tyramide-TMR (donor) and AuNPs-HRP (acceptor) (**Fig. 9A**). In the presence of H_2O_2, the AuNPs-HRP could be directly conjugated with tyramide-TMR and fluorescence quenching occurred because of the energy transfer from tyramide-TMR to AuNPs, which resulted in reduced fluorescence intensity. In contrast, in the absence of H_2O_2, fluorescence quenching did not occur and a strong fluorescence intensity was obtained. In addition to the fluorescence detection, they utilized resonance light scattering correlation spectroscopy (RLSCS), which can

distinguish between AuNPs and AuNP-protein (enzyme) conjugates. To further evaluate the detection system, they checked the relationship between the concentration of the analytes (H_2O_2, glucose, and uric acid) and the TMR fluorescence intensity at 575 nm (**Fig. 9B and 9C**). A prepared solution of H_2O_2, glucose, and uric acid was incubated at room temperature (RT; H_2O_2) and 37 ℃ for 10 min (glucose and uric acid). They used different concentrations of tyramide-TMR and found a linear correlation between the addition of H_2O_2 and the gradual decrease of the fluorescence signal. **Fig. 9B and 9C** present graphs of the relationship between the TMR fluorescence intensity and the glucose and uric acid concentrations, respectively. The TMR fluorescence intensity could be gained in the specific range to evaluate the concentration with detection limit of analytes (concentration range: 0.1-1 μM of glucose and 25-500 nM of uric acid; LOD: 50 nM of glucose and 25 nM of uric acid).

Oligonucleotide detection is another example of molecular diagnostics. For fluorescence quenching from the binding of DNA/RNA to AuNRs, the DNA/RNA should be tagged with fluorescein (FAM) for fluorescent analysis (Lu et al. 2013). FAM is used for the preparation of fluorescein-labeled oligonucleotide probes for the detection of the complementary nucleic acids or primers for polymerase chain reaction. The emission spectrum of FAM is overlap with absorption of the AuNRs and energy transfer can occur from FAM to AuNRs. X. Lu *et al*. have prepared AuNRs-ssDNA (FAM-Labeled DNA) for the detection of target complementary DNA (cDNA). AuNRs were used for the detection of hepatitis B virus (HBV) in their experiment. When the probe DNA (complementary DNA, cDNA) was added into the AuNRs solution (AuNRs with FAM-labeled DNA), the FAM-ssDNA was hybridized with the cDNA to form ds-DNA. Since ds-DNA can have a higher negative charge density than that of ss-FAM-DNA, they can strongly bind to the AuNRs, which enhanced the energy transfer and hence the fluorescence quenching effect. However, if the cDNA is not perfectly matched with FAM-ssDNA, it will not form ds-DNA, which will minimize the energy transfer by AuNRs. The change of fluorescence intensity has been evaluated using probes developed with three different DNA sequences: non-complete complementary sequences (Non), single-base mismatched sequences (A, T, and C), and complete complementary

sequences (G) (**Fig. 10B**). The non-complementary sequences could not be hybridized with the probe DNA, and the value obtained was the lowest among all the sequences. In the case of single-base mismatched sequences, the value obtained was lower than 50% of the perfect complementary sequences. These results suggest that the biosensor could differentiate single-base mismatched DNA sequences from non-complementary and complementary sequences. FAM The biosensor could detect 0.045-6 nM of the cDNA and LOD of 15 pM (signal/noise ratio of 3).

2.3. Electrochemical detection by Au-based Hybrid Materials

Potentiometric sensors measure the change in potential at an electrode compared with a reference electrode. The potential of the working electrode depends on the concentration of each analyte (Koncki 2007). Potentiometric sensors can be broadly classified by the phase of the analytes. For example, the Yttria-stabilized-zirconia (YSZ) oxygen sensor is based on the detection of gas phase mobile ions, using an electrochemical cell related to the auxiliary phase of the chemical species. Among these sensors, the electrode concept is designed for the solution phase of biomolecules in order to increase the feasibility. The most common device is the field effect transistor (FET). These nanometer-scale potentiometric sensors have been developed using single-walled carbon nanotubes (SWCNTs) as field effect sensors (Besteman et al. 2003). Using graphene-like allotropes, carbon nanotubes (CNTs) can be easily adopted for device fabrication due to their high length-to-diameter ratio and their unique electrical properties. Their diameter (~1 nm) is comparable to the size of DNA molecules, which renders them suitable for evaluating the interactions between biomolecules and nanomaterials. The SWCNT-based field effect transistors (SWFETs) can typically detect up to the order of 1 nM in the case of DNA.

To further improve the detection sensitivity, Mhaisalkar and coworkers (Dong et al. 2008) have developed a hybrid system by incorporating AuNPs into the SWFETs. AuNPs, hybridized with the reporter probe DNA strand AAAAAA (6A) or AAAAAAAAAAA (11A), can be selectively matched with the sequence of the target

DNA strand (TTTTTTTTTTT). The inclusion of AuNPs affected the conductivity of the interface electrodes. AuNPs can trigger a negative shift in threshold voltage, which is called the Fermi energy difference between the electrode and CNTs, and which changes the barrier energy of metal-SWNT junctions (Chen et al. 2004; Gui et al. 2007; Tang et al. 2006). Therefore, it contributes to the reduction of the currents showed a 37 % enhancement by reporter DNA-AuNP conjugates. This sensor device notably enhanced the selectivity and sensitivity so can detect up to DNA concentration of 100 fM with a detection range of 100 fM-1 μM. The most important benefit after immobilizing AuNPs is the decrease of source-drain current (Mubeen et al. 2011). These AuNPs on the surface of nanotubes may form localized charge depletion regions, generate charge scattering sites and decrease the hole mobility. The electron donation from AuNPs to SWNTs may increase the SWNTs Fermi level, resulting in greater down-ward band bending of valence and conduction band edges.

Bingjie Cai *et al.* detected miRNA- by decorating AuNPs on the graphene field-effect transistor (FET) (Cai et al. 2015). This graphene FET was fabricated by drop-casting the r-GO and then immersing it in gold precursor ($HAuCl_4$) solution (Dong et al. 2010). They used peptide nucleic acid (PNA) rather than the conventionally used DNA to enhance the selectivity of miRNA detection (Chang et al. 2013). The PNA probe, N-AACCACA-CAACCTACTACCTCA-C, was immobilization on the surface of AuNPs through Au-S bonds. **Fig. 11A** illustrates the scheme of the AuNPs-decorated graphene FET biosensor. When the target miRNAs were introduced for hybridization with probe PNA, they caused an n-doping effect onto the device's currents. The interaction between graphene and electron-rich miRNA (Cai et al. 2014) triggered the leftward-shift of I_{ds}-V_g curves of the devices. **Fig. 11B** shows the transfer of their current decorated with AuNP and immobilized with PNA probe. Comparing the V_{CNP} of the black curve, the red curve obtained after AuNPs decoration was shifted to the right because of the p-doping of AuNPs (Kim et al. 2015). In order to identify the sensitivity of the AuNPs-decorated, graphene-based FET biosensor, various concentrations of complementary miRNAs were introduced to hybridize with PNA immobilized on the FET devices. **Fig. 11C** presents the shift of V_{CNP} after hybridizing with different concentrations of complementary miRNA relative to V_{CNP} of PNA from 1 fM to 100 pM. Not only does the PNA function

as probe, but also the AuNPs can amplify the detection signal. The AuNPs were deposited on the RGO-FET device by dispersion of AuNPs in a mixture of ethanol and water. This method facilitated the formation of very small AuNPs, down to ca.10 nm. The relatively larger surface areas of small AuNPs enables more PNA probes to be immobilized on the AuNPs surface, thus enhancing the sensitivity.

Another example of electrochemical detection methods is amperometric biosensors, in which the resulting electric current caused by an enzyme-catalyzed redox reaction at a working electrode is measured. The most widely used example of redox couples is glucose oxidase (GOx or GOD), which generates hydrogen peroxide and gluconic acid. The hydrogen peroxide is reduced to around -600 mV at the Ag/AgCl anode (reference electrode) (Poyard et al. 1998). The glassy carbon electrode (GCE) was widely used in ideal electrode due to their chemically inert property and low background current. This electrode is usually modified with polymer or catalyst to enhance the detection ability. (Pocard et al. 1992). Typically, AuNPs are labeled with a bio-recognition probe like redox tags or enzymes for the signal generation. Therefore, the capture of AuNPs on the electrode surface can provide numerous electroactive molecules and induce a significant change in the resulting current. The Jin and Shi group (Wei et al. 2010) proposed a more developed model of this GCE by adapting AuNPs. The AuNPs were grown on the surface of ZnO NRs and the ZnO NRs/Au hybrid nanocomposites were attached on GCE. **Fig. 12A** shows a schematic diagram of this GCE structure. **Fig. 12B** shows a current-time plot for this sensor on successive changes of glucose concentration under the 0.55 V potential. This glucose targeting biosensor had detection range of 0.1-33 μM with a detection limit 10 nM. When comparing the absorption peak of the AuNPs and the ZnO NRs/Au hybrid nanocomposite, the latter exhibited a red-shift of the surface plasmon band (520 nm). This change indicates that the interfacial interactions between Au and ZnO trigger a deficient electron density on Au, which confirms the transfer of electrons from Au to ZnO. This composite can transfer electrons between the enzyme and electrode surface more efficiently and exhibited enhanced catalytic activity with GOx (Hashmi and Hutchings 2006). The high conductivity of the ZnO NRs/Au hybrid nanocomposite enhances the direct electron transfer between the active sites of the enzyme and the electrodes. Moreover, the high sensitivity of the enzyme electrode results from the

excellent adsorption ability, enhanced electro-catalytic capability of GOx and good biocompatibility of ZnO NRs/Au hybrid nanocomposite.

In addition, Bai *et al* showed the effect of graphene/AuNR composites in the amperometric device system (Bai et al. 2014). The working electrode, GCE, was modified with graphene/AuNR composite materials under a conventional three-electrode system. The reference electrode was Ag/AgCl and the counter electrode was a platinum wire. Differential pulse voltammetry (DPV) was recorded from -0.6 V to 0.2 V after 3 min accumulation. AuNRs could be tunable and have stronger Vis-NIR absorption, higher surface enhanced Raman scattering cross-sections, and the possibility of unidirectional plasmon propagation (Xu et al. 2011). When the AuNRs were combined with graphene, the simple physical adsorption of AuNPs on graphene afforded the desired structural stability (Muszynski et al. 2008). Owing to the high specific surface area, porosity, and elasticity, as well as chemical stability, graphene has been used as the electrode material for electrochemical sensor devices (Coros et al. 2013). Based on graphene characteristics, AuNRs, which act as the catalyst, could be easily deposited on the surface of graphene (Li et al. 2009). Furthermore, their predominate conductivity helps AuNRs facilitate electron transfer between the immobilized ractopamine and the electrode (Chen et al. 2011). **Fig. 13A** shows a schematic drawing of the synthesis of the graphene/AuNR composite. The mechanism of the oxidation of ractopamine has been discussed in previous studies (Liu et al. 2012). The electrochemical behavior of ractopamine was studied with this conventional three-electrode system: a working electrode of G/AuNR/GCE, reference electrode of Ag/AgCl electrode, and counter electrode of platinum wire. The 3 mm-diameter GCE surface was coated with 8 μL of G/AuNR suspension. The G/AuNR film catalyzed the oxidation of ractopamine, and remarkably raised the response signal of ractopamine. They showed good performance over the range from 1 nM to 2.7 μM with an LOD of 50 fM of ractopamine (**Fig. 13C**).

Lastly, conductometric biosensors recognize the flow of electrical impedance in the ionic medium between the two electrodes. They can detect biomolecular reactions between DNA, proteins, antibodies and so on. These kinds of devices have gained particular attention due to their simple operation and absence of any complicated

reference electrode (Muhammad-Tahir and Alocilja 2003). The information gathered from the ionic strength in electrolytes provides selectivity and sensitivity. In conductometric enzymatic biosensors, the enzyme is cross-linked in surface of electrode then via enzymatic reaction is confined with the presence or absence of NPs. The electrodes interdigitated NPs allow for the change of conductivity to be measured in the region defined by field lines. The observed simultaneous response of the conductometric biosensor can analyze the reaction rate by the kinetics of the enzymatic reaction and the diffusive flux of products away from the transducer surface, in the boundary layer (Temple-Boyer et al. 2008). The widely known enzymatic reaction is pH variation at the transducer surface.

Nouria *et al*. showed the conductometric biosensor structure combined with protease immobilized AuNPs (Nouira et al. 2014). Specifically, proteinase K-coated AuNPs were used as interdigitated electrodes. The conductometric transducer was fabricated from gold deposited ceramic substrate. The interdigital space was 20 μm and the length of the digits was about 1.0 mm. And their surface was modified with crosslinking of proteinase K coated gold nanoparticles (**Fig. 14**). Proteinase K, a serine-based protease, hydrolyzes the peptide specifically located after the hydrophobic amino acids. When this protease hydrolyzes proteins at the surface of the electrode, different ionic amino-acids are produced with the formation of the local conductive charge. Furthermore, the incorporation of AuNPs with a large surface to volume ratio increased the density of the immobilized enzyme and afforded the characteristics of nanoscale electrodes, which are suitable for lowering LOD. The increased conductivity enhanced the detection sensitivity toward a model protein, BSA. The linear range for BSA detection was obtained 0.5-10 mM with an LOD of 0.3 mM.

Another example of conductometric biosensor was introduced by the same group (Nouira et al. 2013). In this case, they synthesized probe materials targeting to glucose. After preparation of polyallylamine hydrochloride (PAH)-coated AuNPs (PAH/AuNPs), GOx was immobilized onto them. The reference electrode of conductometric sensor was modified with resulting hybrid materials. The electrodes were set into glass cells filled with 5 mL of a 5 mM phosphate buffer at pH 7.3. When the solution was stirred

vigorously it acquired a conductance response. Measurements were performed during the application of an alternative voltage (10 mV amplitude, 100 kHz frequency) generated by a low-frequency wave-form generator, which induces reducing Faradaic processes due to double-layer charging and concentration polarization at the microelectrode surface. **Fig. 15B** shows the conductometric measurement after glucose addition. The higher conductance response can be measured at 49 µS for 1 mM glucose concentration. AuNPs effect in amplifying the response of the glucose biosensor, to be sure it, conductometric measurements were performed with GOx-PAH-coated NPs and with directly cross-linked GOx on the conductometric sensor. The experiment was conducted between 0.04 mM and 1 mM to show the relationship between the biosensor response and the glucose concentration. The calibration curve of the glucose sensor measured under the optimum conditions is shown in **Fig. 15C**. In the presence of functionalized AuNPs, the sensitivity is 45 µM/mM, whereas it is only 31 µM/mM when just directly cross-linked on the conductometric sensor. The LOD was 50 µM of glucose when GOx was directly deposited on the top of the IDEs. In contrast, LOD of 9 µM glucose was recorded when GOx-functionalized AuNPs were deposited on top of the IDEs.

3. Conclusion and Future perspectives

In summary, gold-based hybrid nanomaterials provide promising features in molecular diagnostics by continuously enhancing the LOD of biosensors. As previously described, gold nanomaterials and their hybrids have shown various unique advantages. On their own, gold nanomaterials have controllable optical property, good compatibility with various ligands, and abundant electrons. In addition, when they are combined with other functional materials such as proteins, oligonucleotides, polymers, GO sheets, and inorganic materials, the resulting hybrids can offer superior detection sensitivity over conventional detection methods while reducing the analysis time and the LOD. The diverse choice of hybrids formed by combining gold nanomaterials and functional macromolecules has further broadened their potential utility. Novel gold-based hybrid

nanomaterials for diagnostic applications continue to emerge and many ingenious detection systems with far superior detection capabilities have been developed by applying these materials.

Various future efforts will have to be made to take full advantage of the versatile properties of gold-based hybrid nanomaterials. This will include the development of fast, label-free, highly sensitive, and real-time multiplexed molecular diagnostics in automated fashion. The cost-effectiveness aspect is also to be taken into account when it comes to detection and diagnosis methods. After the proper establishment of such systems assuring fast and reproducible biosensing, we can easily imagine the application of these devices for the provision of facile and routine health checks at home, thereby facilitating the detection of any abnormalities at an early stage. It is also important that, during the development of new generation, gold-based hybrid nanomaterials, the protocols and results need to be well validated as compared to the existing clinical diagnosis methods in order to gain market acceptance. This is particularly of interest to the industry, since many of novel biosensors fail to satisfy the regulatory guidelines for the in vitro biosensors. Moreover, most of the chips and biosensing tools described in this review are used in the diagnostic detection of biomarkers outside the body. There remain limitations and challenges of in vitro diagnostics that cannot cover the complexity of intact organ systems. Therefore, they do not allow the simultaneous and continues monitoring of in vivo disease state. The need for the development of in vivo sensors has been discussed earlier; however, their biocompatibility and pharmacokinetic properties remain indefinable and have not yet fully elucidated (Kuchimaru et al. 2010; Lama et al. 2012; Stefflova et al. 2006). Especially, 1) keeping the living system intact and 2) the low sensitivity of in vivo sensors are currently major issues to be overcome (Scheller et al. 2001). Only few current studies have examined the clinical utilization of gold-based hybrid nanomaterials for in vivo and real-time biosensing (Singh et al. 2012).

In this review, we have tried to comprehensively overview the past, present, and future of gold nanomaterial-based biosensors and diagnostic tools, and the impact of gold-based hybrid nanomaterials on biosensors. It is believed that the rapid development and market introduction of these gold-based hybrid nanomaterials will be assisted by such studies

following a multidisciplinary approach. By introducing the primary developments of novel gold-based hybrid nanomaterials, their device structures, and functionalities, our review has highlighted the significant milestones achieved by gold nanomaterial-based biosensors and further elucidated the emerging future prospects in this field.

4. Acknowledgment

J.E.K., J.H.C., M.C. contributed equally to this work. This work was supported by the Basic Science Research Program (2015R1A1A1A05027352, H. Lee), the Biomedical Technology Development Program (2015M3A9D7031026, H. Lee), and the Mid-career Researcher Program through National Research Foundation of Korea Grant funded by the Ministry of Education and Science Technology (2014R1A2A1A09005656, D. H. Kim).

5. References

Anker, J.N., Hall, W.P., Lyandres, O., Shah, N.C., Zhao, J., Van Duyne, R.P., 2008. Nat. Mater. 7(6), 442-453.

Asangani, I.A., Rasheed, S.A.K., Nikolova, D.A., Leupold, J.H., Colburn, N.H., Post, S., Allgayer, H., 2007. Oncogene 27(15), 2128-2136.

Bai, W., Huang, H., Li, Y., Zhang, H., Liang, B., Guo, R., Du, L., Zhang, Z., 2014. Electrochim. Acta 117, 322-328.

Banholzer, M.J., Millstone, J.E., Qin, L., Mirkin, C.A., 2008. Chem. Soc. Rev. 37(5), 885-897.

Besteman, K., Lee, J.-O., Wiertz, F.G.M., Heering, H.A., Dekker, C., 2003. Nano Lett. 3(6), 727-730.

Bi, S., Yan, Y., Yang, X., Zhang, S., 2009. Chemistry – A European Journal 15(18), 4704-4709.

Boisselier, E., Astruc, D., 2009. Chemical Society Reviews 38(6), 1759-1782.

Borriello, A., Agoretti, P., Cassinese, A., D'Angelo, P., Mohanraj, G., Sanguigno, L., 2009. Journal of nanoscience and nanotechnology 9(11), 6307-6314.

Bottoni, A., Piccin, D., Tagliati, F., Luchin, A., Zatelli, M.C., Degli Uberti, E.C., 2005. J. Cell. Physiol. 204(1), 280-285.

Bunz, U.F., 2005. Synthesis and Structure of PAEs. In: Weder, C. (Ed.), Poly(arylene etynylene)s, pp. 1-52. Springer Berlin Heidelberg.

Cai, B., Huang, L., Zhang, H., Sun, Z., Zhang, Z., Zhang, G.-J., 2015. Biosens. Bioelectron. 74, 329-334.

Cai, B., Wang, S., Huang, L., Ning, Y., Zhang, Z., Zhang, G.-J., 2014. ACS nano 8(3), 2632-2638.

Cao, J., Sun, T., Grattan, K.T.V., 2014. Sensors and Actuators B: Chemical 195, 332-351.

Chan, J.A., Krichevsky, A.M., Kosik, K.S., 2005. Cancer Res. 65(14), 6029-6033.

Chang, J., Mao, S., Zhang, Y., Cui, S., Zhou, G., Wu, X., Yang, C.-H., Chen, J., 2013. Nanoscale 5(9), 3620-3626.

Chateau, D., Liotta, A., Vadcard, F., Navarro, J.R.G., Chaput, F., Lerme, J., Lerouge, F., Parola, S., 2015. Nanoscale 7(5), 1934-1943.

Chen, L., Neethirajan, S., 2015. Sensors 15(4), 8852.

Chen, N.-T., Cheng, S.-H., Liu, C.-P., Souris, J., Chen, C.-T., Mou, C.-Y., Lo, L.-W., 2012. International Journal of Molecular Sciences 13(12), 16598.

Chen, P., Chung, M.T., McHugh, W., Nidetz, R., Li, Y., Fu, J., Cornell, T.T., Shanley, T.P., Kurabayashi, K., 2015. ACS Nano 9(4), 4173-4181.

Chen, R.J., Choi, H.C., Bangsaruntip, S., Yenilmez, E., Tang, X., Wang, Q., Chang, Y.-L., Dai, H., 2004. J. Am. Chem. Soc. 126(5), 1563-1568.

Chen, Y., Li, Y., Sun, D., Tian, D., Zhang, J., Zhu, J.-J., 2011. J. Mater. Chem. 21(21), 7604-7611.

Cheng, L., Song, J., Yin, J., Duan, H., 2011. The Journal of Physical Chemistry Letters 2(17), 2258-2262.

Cheng, W., Dong, S., Wang, E., 2003. Angew. Chem. Int. Ed. 42(4), 449-452.

Cheng, W., Jiang, J., Dong, S., Wang, E., 2002. Chem. Commun.(16), 1706-1707.

Chiu, T.-C., Huang, C.-C., 2009. Sensors 9(12), 10356-10388.

Coros, M., Biris, A.R., Pogacean, F., Tudoran, L.B., Neamtu, C., Watanabe, F., Biris, A.S., Pruneanu, S., 2013. Electrochim. Acta 91, 137-143.

Dillhoff, M., Liu, J., Frankel, W., Croce, C., Bloomston, M., 2008. J Gastrointest Surg 12(12), 2171-2176.

Dong, X., Lau, C.M., Lohani, A., Mhaisalkar, S.G., Kasim, J., Shen, Z., Ho, X., Rogers, J.A., Li, L.-J., 2008. Advanced Materials 20(12), 2389-2393.

Dong, X., Shi, Y., Huang, W., Chen, P., Li, L.J., 2010. Adv. Mater. 22(14), 1649-1653.

dos Remedios, C.G., Moens, P.D.J., 1995. Journal of Structural Biology 115(2), 175-185.

Félidj, N., Laurent, G., Grand, J., Aubard, J., Lévi, G., Hohenau, A., Aussenegg, F., Krenn, J., 2006. Plasmonics 1(1), 35-39.

Fabris, L., Dante, M., Braun, G., Lee, S.J., Reich, N.O., Moskovits, M., Nguyen, T.-Q., Bazan, G.C., 2007. J. Am. Chem. Soc. 129(19), 6086-6087.

Fan, C., Wang, S., Hong, J.W., Bazan, G.C., Plaxco, K.W., Heeger, A.J., 2003. Proceedings of the National Academy of Sciences 100(11), 6297-6301.

Fan, W., Lee, Y.H., Pedireddy, S., Zhang, Q., Liu, T., Ling, X.Y., 2014. Nanoscale 6(9), 4843-4851.

Fang, C., Fan, Y., Kong, J., Gao, Z., Balasubramanian, N., 2008. Anal. Chem. 80(24), 9387-9394.

Ghosh, D., Chattopadhyay, N., 2013. Optics and Photonics Journal 3(01), 18-26.

Griffin, J., Singh, A.K., Senapati, D., Rhodes, P., Mitchell, K., Robinson, B., Yu, E., Ray, P.C., 2009. Chemistry – A European Journal 15(2), 342-351.

Gui, E.L., Li, L.-J., Zhang, K., Xu, Y., Dong, X., Ho, X., Lee, P.S., Kasim, J., Shen, Z.X., Rogers, J.A., Mhaisalkar, 2007. J. Am. Chem. Soc. 129(46), 14427-14432.

Haes, A.J., Zou, S., Schatz, G.C., Van Duyne, R.P., 2004. The Journal of Physical Chemistry B 108(22), 6961-6968.

Hashmi, A.S.K., Hutchings, G.J., 2006. Angew. Chem. 118(47), 8064-8105.

Haynes, C.L., Van Duyne, R.P., 2003. The Journal of Physical Chemistry B 107(30), 7426-7433.

He, H., Xie, C., Ren, J., 2008. Analytical Chemistry 80(15), 5951-5957.

Hu, C.-W., Huang, Y., Tsiang, R.C.-C., 2009. Journal of nanoscience and nanotechnology 9(5), 3084-3091.

Hu, Y., Zhang, L., Zhang, Y., Wang, B., Wang, Y., Fan, Q., Huang, W., Wang, L., 2015. ACS Applied Materials & Interfaces 7(4), 2459-2466.

Huang, H.J., Yu, C.-p., Chang, H.C., Chiu, K.P., Ming Chen, H., Liu, R.S., Tsai, D.P., 2007. Opt. Express 15(12), 7132-7139.

Huang, X., Lan, T., Zhang, B., Ren, J., 2012. Analyst 137(16), 3659-3666.

Huang, Y., Chen, J., Shi, M., Zhao, S., Chen, Z.-F., Liang, H., 2013. Journal of Materials Chemistry B 1(15), 2018-2021.

Ikami, M., Kawakami, A., Kakuta, M., Okamoto, Y., Kaji, N., Tokeshi, M., Baba, Y., 2010. Lab Chip 10(24), 3335-3340.

Jalani, G., Cerruti, M., 2015. Nanoscale 7(22), 9990-9997.

Jiang, W., KimBetty, Y.S., Rutka, J.T., ChanWarren, C.W., 2008. Nat Nano 3(3), 145-150.

Kim, D.Y., Yu, T., Cho, E.C., Ma, Y., Park, O.O., Xia, Y., 2011. Angew. Chem. Int. Ed. 50(28), 6328-6331.

Kim, I.-B., Dunkhorst, A., Gilbert, J., Bunz, U.H.F., 2005. Macromolecules 38(11), 4560-4562.

Kim, J.-W., Galanzha, E.I., Shashkov, E.V., Moon, H.-M., Zharov, V.P., 2009. Nat Nano 4(10), 688-694.

Kim, K.W., Song, W., Jung, M.W., Kang, M.-A., Kwon, S.Y., Myung, S., Lim, J., Lee, S.S., An, K.-S., 2015. Carbon 82, 96-102.

Kim, S.K., Cho, H., Jeong, J., Kwon, J.N., Jung, Y., Chung, B.H., 2010. Chem. Commun. 46(19), 3315-3317.

Kodama, T., Jain, A., Goodson, K.E., 2009. Nano Lett. 9(5), 2005-2009.

Koncki, R., 2007. Anal. Chim. Acta 599(1), 7-15.

Kuchimaru, T., Kadonosono, T., Tanaka, S., Ushiki, T., Hiraoka, M., Kizaka-Kondoh, S., 2010. PloS one 5(12), e15736.

Lama, R.D., Charlson, K., Anantharam, A., Hashemi, P., 2012. Anal. Chem. 84(19), 8096-8101.

Lee, H., Lee, K., Kim, I.-K., Park, T.G., 2009. Advanced Functional Materials 19(12), 1884-1890.

Li, C.M., Li, Y.F., Wang, J., Huang, C.Z., 2010. Talanta 81(4–5), 1339-1345.

Li, M., Cushing, S.K., Wu, N., 2015. Analyst 140(2), 386-406.

Li, M., Cushing, S.K., Zhang, J., Lankford, J., Aguilar, Z.P., Ma, D., Wu, N., 2012. Nanotechnology 23(11), 115501.

Li, Y., Tang, L., Li, J., 2009. Electrochem. Commun. 11(4), 846-849.

Lilley, D.M.J., Wilson, T.J., 2000. Current Opinion in Chemical Biology 4(5), 507-517.

Liu, J., Yang, X., He, X., Wang, K., Wang, Q., Guo, Q., Shi, H., Huang, J., Huo, X., 2011. Sci. China Chem. 54(8), 1157-1176.

Liu, Y., Li, Y., He, J., Duelge, K.J., Lu, Z., Nie, Z., 2014. J. Am. Chem. Soc. 136(6), 2602-2610.

Liu, Z., Zhou, Y., Wang, Y., Cheng, Q., Wu, K., 2012. Electrochim. Acta 74, 139-144.

Lu, X., Dong, X., Zhang, K., Han, X., Fang, X., Zhang, Y., 2013. Analyst 138(2), 642-650.

Mühlschlegel, P., Eisler, H.-J., Martin, O., Hecht, B., Pohl, D., 2005. Science 308(5728), 1607-1609.

Mayer, K.M., Hafner, J.H., 2011. Chem. Rev. 111(6), 3828-3857.

Meng, F., Henson, R., Wehbe–Janek, H., Ghoshal, K., Jacob, S.T., Patel, T., 2007. Gastroenterology 133(2), 647-658.

Moon, H., Kumar, D., Kim, H., Sim, C., Chang, J.-H., Kim, J.-M., Kim, H., Lim, D.-K., 2015. ACS nano 9(3), 2711-2719.

Mubeen, S., Lim, J.H., Srirangarajan, A., Mulchandani, A., Deshusses, M.A., Myung, N.V., 2011. Electroanalysis 23(11), 2687-2692.

Muhammad-Tahir, Z., Alocilja, E.C., 2003. Biosens. Bioelectron. 18(5), 813-819.

Muszynski, R., Seger, B., Kamat, P.V., 2008. The Journal of Physical Chemistry C 112(14), 5263-5266.

Nehl, C.L., Liao, H., Hafner, J.H., 2006. Nano Lett. 6(4), 683-688.

Ng, K.C., Udagedara, I.B., Rukhlenko, I.D., Chen, Y., Tang, Y., Premaratne, M., Cheng, W., 2012. ACS Nano 6(1), 925-934.

Nouira, W., Maaref, A., Elaissari, H., Vocanson, F., Siadat, M., Jaffrezic-Renault, N., 2013. Materials Science and Engineering: C 33(1), 298-303.

Nouira, W., Maaref, A., Elaissari, H., Vocanson, F., Siadat, M., Jaffrezic-Renault, N., 2014. Sensors 14(7), 13298-13307.

Oh, E., Hong, M.-Y., Lee, D., Nam, S.-H., Yoon, H.C., Kim, H.-S., 2005. Journal of the American Chemical Society 127(10), 3270-3271.

Ongaro, A., Griffin, F., Nagle, L., Iacopino, D., Eritja, R., Fitzmaurice, D., 2004. Adv. Mater. 16(20), 1799-1803.

Ono, A., Kato, J.-i., Kawata, S., 2005. Phys. Rev. Lett. 95(26), 267407.

Park, J.-H., Byun, J.-Y., Mun, H., Shim, W.-B., Shin, Y.-B., Li, T., Kim, M.-G., 2014. Biosens. Bioelectron. 59, 321-327.

Parkhurst, L.J., Parkhurst, K.M., Powell, R., Wu, J., Williams, S., 2002. Biopolymers 61(3), 180-200.

Pocard, N.L., Alsmeyer, D.C., McCreery, R.L., Neenan, T.X., Callstrom, M.R., 1992. J. Mater. Chem. 2(8), 771-784.

Poyard, S., Jaffrezic-Renault, N., Martelet, C., Cosnier, S., Labbe, P., 1998. Anal. Chim. Acta 364(1), 165-172.

Qin, C., Wen, W., Zhang, X., Gu, H., Wang, S., 2015a. Chem. Commun. 51(39), 8273-8275.

Qin, L., He, X., Chen, L., Zhang, Y., 2015b. ACS Applied Materials & Interfaces 7(10), 5965-5971.

Quintela, I.A., Benildo, G., Lin, C.-S., Wu, V.C., 2015. Nanoscale 7(6), 2417-2426.

Ray, C.A., Bowsher, R.R., Smith, W.C., Devanarayan, V., Willey, M.B., Brandt, J.T., Dean, R.A., 2005. J. Pharm. Biomed. Anal. 36(5), 1037-1044.

Reddaiah, K., Madhusudana Reddy, T., 2014. J. Mol. Liq. 196, 77-85.

Sönnichsen, C., Alivisatos, A.P., 2005. Nano Lett. 5(2), 301-304.

Samanta, A., Zhou, Y., Zou, S., Yan, H., Liu, Y., 2014. Nano Letters 14(9), 5052-5057.

Samanta, S., Locklin, J., 2008. Langmuir 24(17), 9558-9565.

Schöller, K., Küpfer, S., Baumann, L., Hoyer, P.M., de Courten, D., Rossi, R.M., Vetushka, A., Wolf, M., Bruns, N., Scherer, L.J., 2014. Adv. Funct. Mater. 24(33), 5194-5201.

Scheller, F.W., Wollenberger, U., Warsinke, A., Lisdat, F., 2001. Curr. Opin. Biotechnol. 12(1), 35-40.

Seidel, J., Baida, F.I., Bischoff, L., Guizal, B., Grafström, S., Van Labeke, D., Eng, L.M., 2004. Physical Review B 69(12), 121405.

Sekar, R.B., Periasamy, A., 2003. The Journal of Cell Biology 160(5), 629-633.

Selvin, P.R., 2000. Nat Struct Mol Biol 7(9), 730-734.

Setsukinai, K.-i., Urano, Y., Kakinuma, K., Majima, H.J., Nagano, T., 2003. Journal of Biological Chemistry 278(5), 3170-3175.

Singh, S., Srivastava, A., Oh, H.-M., Ahn, C.-Y., Choi, G.-G., Asthana, R.K., 2012. Toxicon 60(5), 878-894.

Song, J., Cheng, L., Liu, A., Yin, J., Kuang, M., Duan, H., 2011. J. Am. Chem. Soc. 133(28), 10760-10763.

Song, Y., Zhao, C., Ren, J., Qu, X., 2009. Chem. Commun.(15), 1975-1977.

Stefflova, K., Chen, J., Li, H., Zheng, G., 2006. Molecular imaging 5(4), 520.

Storhoff, J.J., Lucas, A.D., Garimella, V., Bao, Y.P., Muller, U.R., 2004. Nat Biotech 22(7), 883-887.

Swager, T., Zheng, J., 2005. Poly(arylene ethynylene)s in Chemosensing and Biosensing. In: Weder, C. (Ed.), Poly(arylene etynylene)s, pp. 151-179. Springer Berlin Heidelberg.

Takamizawa, J., Konishi, H., Yanagisawa, K., Tomida, S., Osada, H., Endoh, H., Harano, T., Yatabe, Y., Nagino, M., Nimura, Y., 2004. Cancer Res. 64(11), 3753-3756.

Tan, L., Zeng, M., Wu, Q., Chen, L., Wang, J., Zhang, T., Eckert, J., Rümmeli, M.H., Fu, L., 2015. Small 11(15), 1840-1846.

Tang, X., Bansaruntip, S., Nakayama, N., Yenilmez, E., Chang, Y.-l., Wang, Q., 2006. Nano Lett. 6(8), 1632-1636.

Tao, H., Liao, X., Xu, M., Xie, X., Zhong, F., Yi, Z., 2014. Analytical Methods 6(8), 2560-2565.

Taton, T.A., Mirkin, C.A., Letsinger, R.L., 2000. Science 289(5485), 1757-1760.

Temple-Boyer, P., Benyahia, A., Sant, W., Pourciel-Gouzy, M., Launay, J., Martinez, A., 2008. Sensors and Actuators B: Chemical 131(2), 525-532.

Wang, G., Stender, A.S., Sun, W., Fang, N., 2010. Analyst 135(2), 215-221.

Wang, J.-Y., Wang, X.-L., Liu, P., 1999. World Journal of Gastroenterology 5, 38-40.

Wang, J., Wang, K., Bartling, B., Liu, C.-C., 2009. Sensors 9(11), 8709.

Wang, L.V., Hu, S., 2012. Science 335(6075), 1458-1462.

Wang, P., Zhang, W., Liang, O., Pantoja, M., Katzer, J., Schroeder, T., Xie, Y.-H., 2012. ACS Nano 6(7), 6244-6249.

Wang, X., Pang, Y., Ku, G., Xie, X., Stoica, G., Wang, L.V., 2003. Nat Biotech 21(7), 803-806.

Wei, Y., Li, Y., Liu, X., Xian, Y., Shi, G., Jin, L., 2010. Biosens. Bioelectron. 26(1), 275-278.

Wijaya, A., Schaffer, S.B., Pallares, I.G., Hamad-Schifferli, K., 2009. ACS Nano 3(1), 80-86.

Wittenberg, N.J., Haynes, C.L., 2009. Wiley Interdisciplinary Reviews: Nanomedicine and Nanobiotechnology 1(2), 237-254.

Xu, C.S., Cang, H., Montiel, D., Yang, H., 2007. The Journal of Physical Chemistry C 111(1), 32-35.

Xu, L., Kuang, H., Wang, L., Xu, C., 2011. J. Mater. Chem. 21(42), 16759-16782.

Xu, W., Xiao, J., Chen, Y., Chen, Y., Ling, X., Zhang, J., 2013. Adv. Mater. 25(6), 928-933.

Yang, C., Wang, Y., Marty, J.-L., Yang, X., 2011. Biosens. Bioelectron. 26(5), 2724-2727.

Yi, Z., Li, X.-Y., Liu, F.-J., Jin, P.-Y., Chu, X., Yu, R.-Q., 2013. Biosens. Bioelectron. 43, 308-314.

You, C.-C., Miranda, O.R., Gider, B., Ghosh, P.S., Kim, I.-B., Erdogan, B., Krovi, S.A., Bunz, U.H.F., Rotello, V.M., 2007. Nat Nano 2(5), 318-323.

Yue, Z., Lisdat, F., Parak, W.J., Hickey, S.G., Tu, L., Sabir, N., Dorfs, D., Bigall, N.C., 2013. ACS Applied Materials & Interfaces 5(8), 2800-2814.

Zhang, J., Ting, B.P., Jana, N.R., Gao, Z., Ying, J.Y., 2009. Small 5(12), 1414-1417.

Zhang, L., Dai, L., Rong, Y., Liu, Z., Tong, D., Huang, Y., Chen, T., 2015a. Langmuir 31(3), 1164-1171.

Zhang, Y.-F., Yang, D.-J., Wang, J.-H., Wang, Y.-L., Ding, S.-J., Zhou, L., Hao, Z.-H., Wang, Q.-Q., 2015b. Nanoscale 7(18), 8503-8509.

Zhao, J., Dieringer, J.A., Zhang, X., Schatz, G.C., Van Duyne, R.P., 2008. The Journal of Physical Chemistry C 112(49), 19302-19310.

Zheng, P., Li, M., Jurevic, R., Cushing, S.K., Liu, Y., Wu, N., 2015a. Nanoscale 7(25), 11005-11012.

Zheng, W., Tu, D., Huang, P., Zhou, S., Chen, Z., Chen, X., 2015b. Chem. Commun. 51(20), 4129-4143.

Zhu, Y., Murali, S., Cai, W., Li, X., Suk, J.W., Potts, J.R., Ruoff, R.S., 2010. Adv. Mater. 22(35), 3906-3924.

Table 1

Gold-based hybrid materials for biosensor and their LOD comparison

Detection Method	Type of Materials	Target of Analytes	Concentration range / LOD	Ref.
Optical Detection	AuNP-ssDNA	miRNA	10 nM-20 μM / 3 nM	(Hu et al. 2015)
	AuNR-Antibody	Cytokines	10-10000 ng L^{-1} / 10 ng L^{-1}	(Chen et al. 2015)
	HO-AuNP-DNA	Proteins	5 pg-20 μg L^{-1} / 2.9 μg L^{-1}	(Qin et al. 2015a)
	AuNP	DNA	10 pM-100 nM / 10 pM	(Kim et al. 2010)
	AuNP-DNA	DNA	10-1000 CFU mL^{-1} / 10 CFU mL^{-1}	(Quintela et al. 2015)
	AuNR-Aptamer	Ochratoxin A	1 nM-1 μM / 0.1 nM-10 μM	(Park et al. 2014)
	AuNP	DNA	0-300 nM / 10 nM	(Yi et al. 2013)
		Hg^{2+}	0-3.0 μM / 0.2 μM	
	AuNS-silica shell	Ag^{+}	2 pM-10 nM / 1.7 pM	(Zheng et al. 2015a)
		Hg^{2+}	5 pM-100 nM / 2.3 pM	
Fluorescence Detection	AuNR-Antibody	hIgG	4-220 mg L^{-1} / 8.3 mg L^{-1}	(Tao et al. 2014)
	AuNP-Antibody	H5N1	1 pM-10 nM / 38 pM-12 nM	(Chen and Neethirajan 2015)
	AuNP-HA	$^{\cdot}O_2^{-}$	1-100 μM / 20 μM	(Lee et al. 2009)
		$^{\cdot}OH$	1-100 μM / 5 μM	
	AuNR-DNA	HBV	0.045-6 nM / 15 pM	(Lu et al. 2013)

	AuNP-RNA	HCV	15-550 pM / 300 fM	(Griffin et al. 2009)
	AuNC-AuNR	GST	2-100 nM / 1.5 nM	(Qin et al. 2015b)
	AuNP-HRP (AuNP-BSA)	H_2O_2	25-400 nM / 10 nM	(Huang et al. 2012)
		Glucose	0.1-1 µM / 50 nM	
		Uric acid	25-500 nM / 25 nM	
Eletro-chemical Detection	AuNP-DNA	DNA	1 fM-100 pM / 1 fM	(Dong et al. 2008)
	AuNP-PNA	miRNA	1 fM-100 pM / 1 fM	(Cai et al. 2015)
	AuNP-ZnO	Glucose	0.1-33 µM / 10 nM	(Wei et al. 2010)
	AuNR-Graphene	Ractopamine	0.001–2.7 µM / 50 fM	(Bai et al. 2014)
	AuNP-Protease	BSA	0.5-10 mg L^{-1} / 0.3 mg L^{-1}	(Wang et al. 2009)
	AuNP-GOx (AuNP-GOD)	Glucose	0.04 mM-1 mM / 9 µM	(Nouira et al. 2013)

Abbreviations: LOD, limit of detection; AuNP, gold nanoparticle; ssDNA, single-strand DNA; miRNA, microRNA; AuNR, gold nanorod; hIgG, human immunoglobulin G; H5N1, influenza A virus subtype H5N1 ; HA, hyaluronic acid; AuNC, gold nanocluster; HBV, hepatitis B virus; HCV, hepatitis C virus; GST, glutathione S-transferase; HRP, horseradish peroxidase; BSA, bovine serum albumin; PNA, peptide nucleic acid; GOx or GOD, glucose oxidase

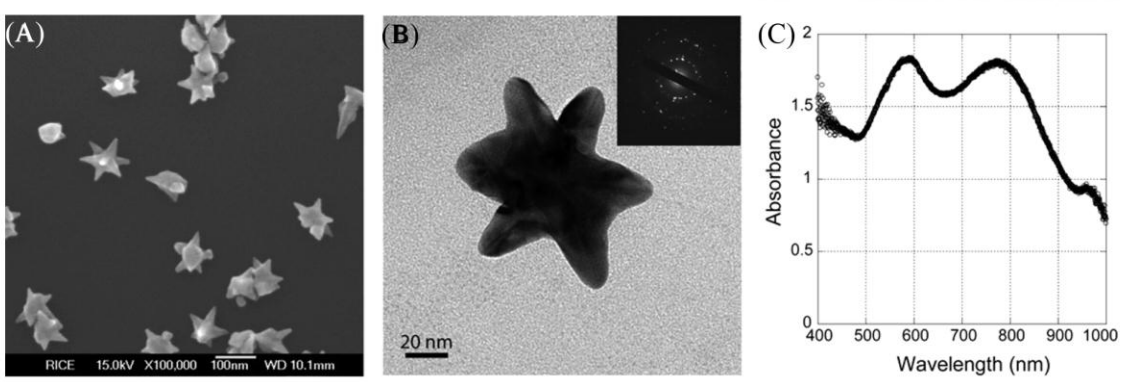

Fig. 1. (A) SEM image of star-shaped AuNPs showing the heterogeneity of shapes obtained after synthesis. (B) TEM image and electron diffraction of a NS showing multiple crystal domains. (C) Extinction spectrum of a NS solution, showing peaks in both visible and near infrared region 25-500 nM.

(Reprinted with permission from (Nehl et al., 2006). Copyright © 2006, American Chemical Society)

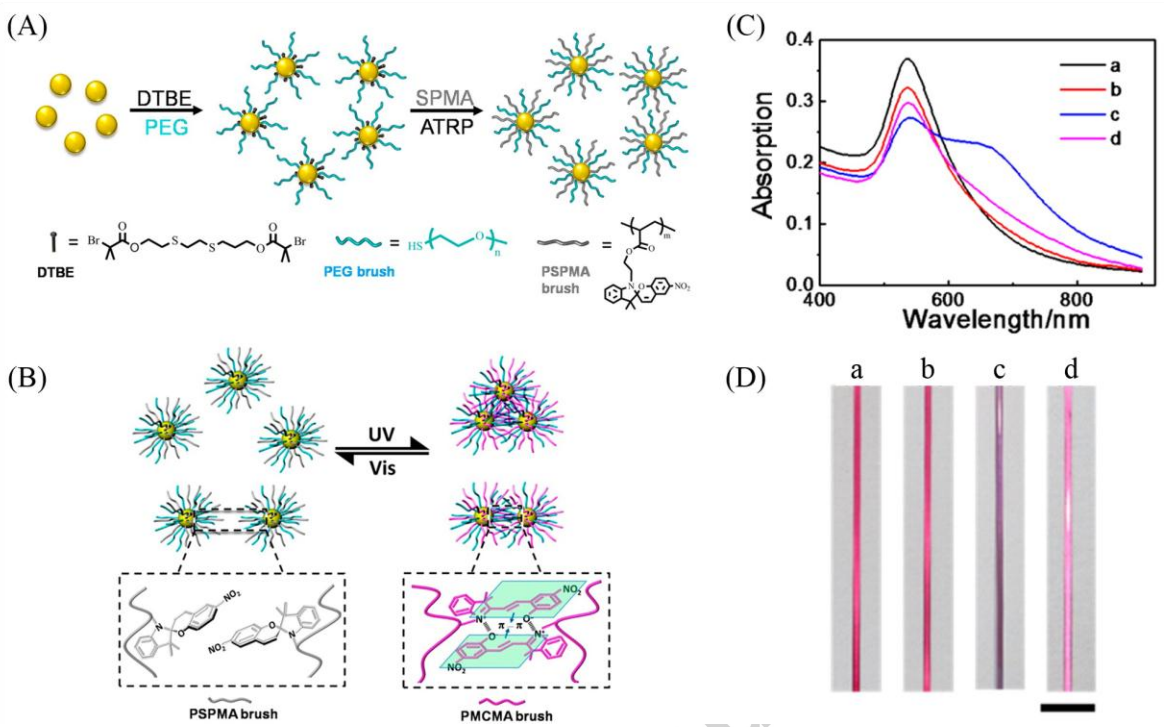

Fig. 2. (A) Schematic representation of amphiphilic Au-PEG/PSPMA synthesis (functionalization of AuNPs by PEG and PSPMA). (B) Reversible assembly and disassembly of the Au oligomers under UV and visible light. (C) UV-vis absorption spectrum of an Au-PEG/PSPMA solution (a: in DMF; b: after H_2O addition; c: after UV light irradiation; d: after visible light exposure showing the reversibility of the process). (D) Photographs of the solutions in capillary (scale bar: 1cm)

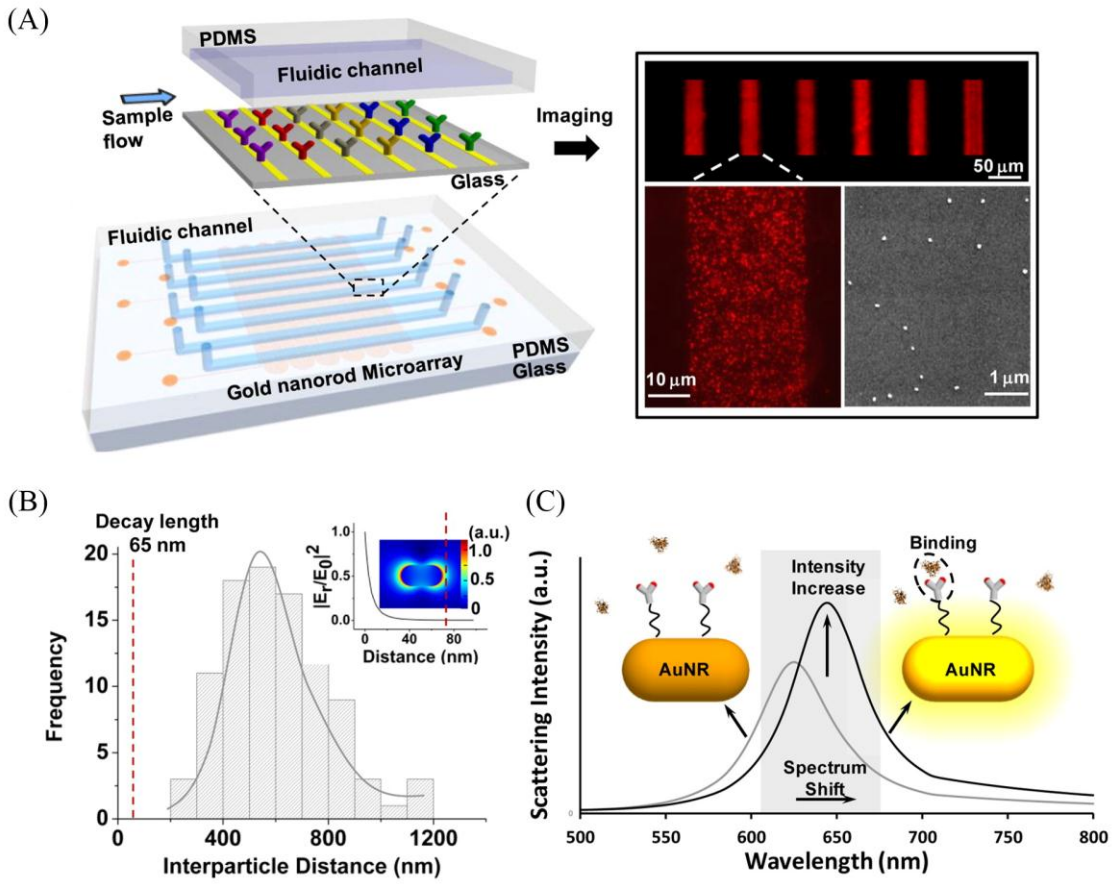

Fig. 3. (A) Schematic representation of the LSPR chip, incorporating microfluidic channels with AuNRs by electrostatic interactions with the substrate surface. Antibodies were attached onto AuNRs using thiolated cross-linker. The chip was imaged under dark-field microscopy and SEM. (B) Histogram of the interparticle distance in the chip calculated using SEM images. (C) Principle of the LSPR microarray chip method, showing the SPR spectrum and the red-shift occurring when antibodies bind to their probe.

(Reprinted with permission from (Chen et al., 2015). Copyright © 2015, American Chemical Society)

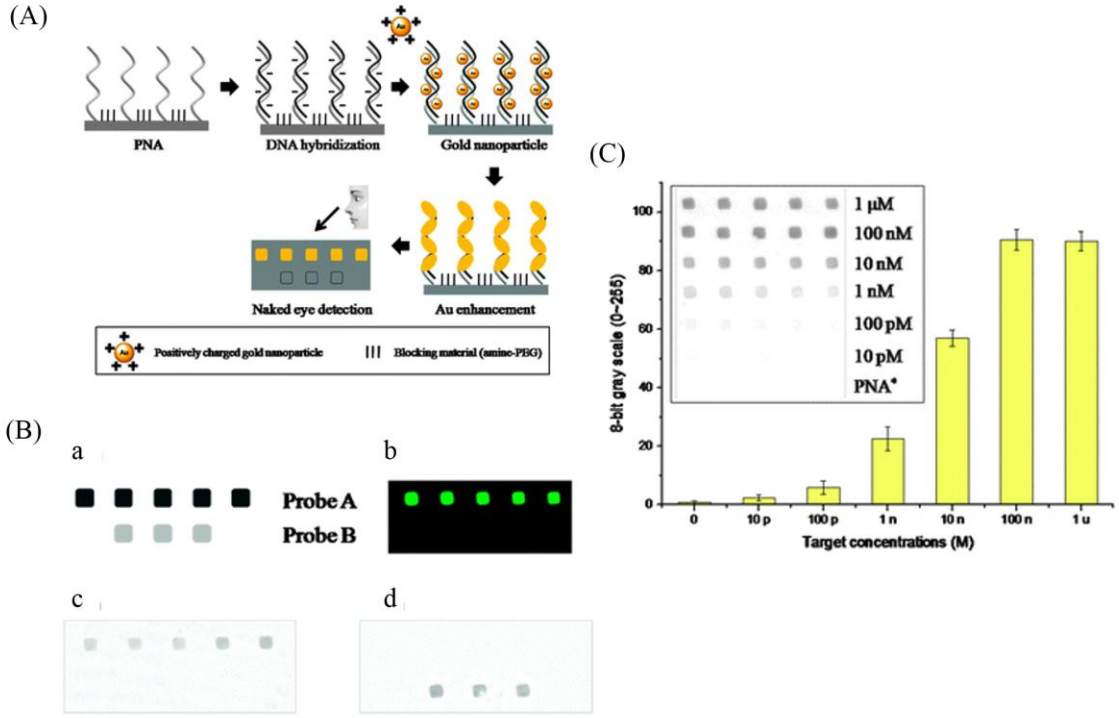

Fig. 4. (A) Schematic representation of the detection method: negatively charged DNA hybridizes with complementary neutral PNA, and positively charged AuNPs bind to the probe DNA for naked eye or optical scanner detection. (B) Grayscale response of AuNPs depending on their size, the highest difference level between the spot and background occurred for 4 nm particles so they were chosen as the optimal AuNP for detection. (C) Fluorescent (b), optical scanner (c) and (d) images of the chip spotted with probe A and B (a), and the results obtained when applying A target or B target. (D) Grayscale values depending on the target concentrations and on the inset: optical scanner images of different target concentrations.

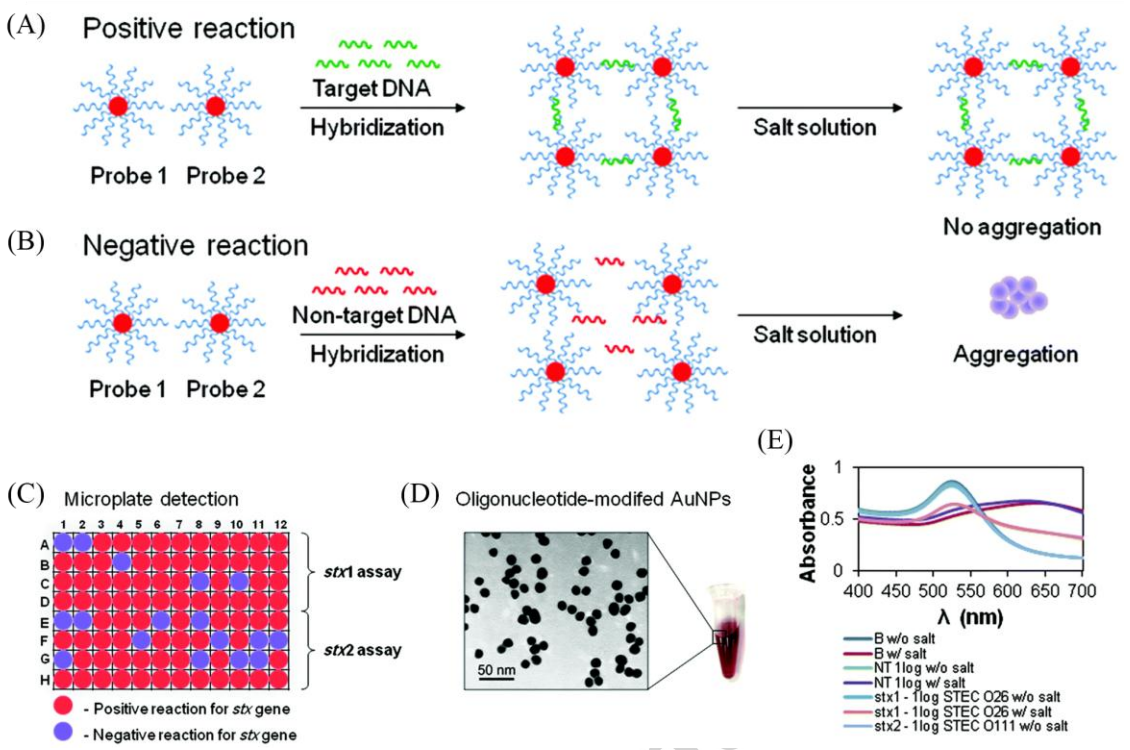

Fig. 5. Schematic representations of the device and its principle. (A) Sandwich hybridization between both probes and target DNA forming a stable complex resistant to high salt concentrations and so maintaining its red color. (B) Negative reaction when non-target DNA is added to the plate. Hybridization does not occur, leading to aggregation of the AuNPs under high salt concentrations, and a color change to purplish-blue. (C) Resulting color changes in the plate. (D) TEM image of the AuNP with oligonucleotides attached. (E) Absorbance spectrum of each sample, before and after salt addition (B: blank; NT: non-target), showing a similar peak for the target DNA, whether or not salt is added to the sample.

(Reprinted with permission from (Quintela et al., 2015). Copyright © 2014, Royal Society of Chemistry)

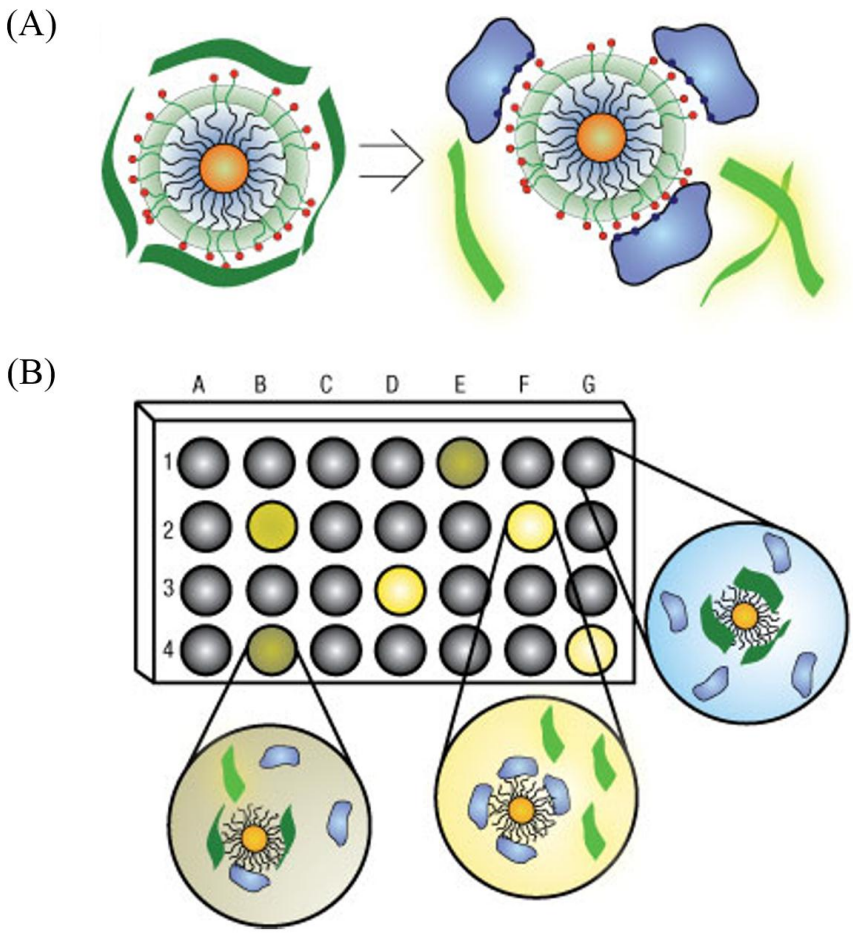

Fig. 6. Schematic illustration of fluorophore displacement protein sensor array. (A) Displacement of quenched fluorescent polymer (dark green: fluorescence off; light green strips: fluorescence on) by protein analyte (blue) with concomitant restoration of fluorescence. The particle monolayers afford the properties of a stable hydrophobic core, a biocompatible oligo(ethylene glycol) layer is, and surface charged residues that can interact with proteins. (B) Fluorescence pattern generation through differential release of fluorescent polymers from AuNPs. The wells of the microplates contain different AuNPs-polymer conjugates, and the addition of protein analytes produces a specific indicator for a given protein.

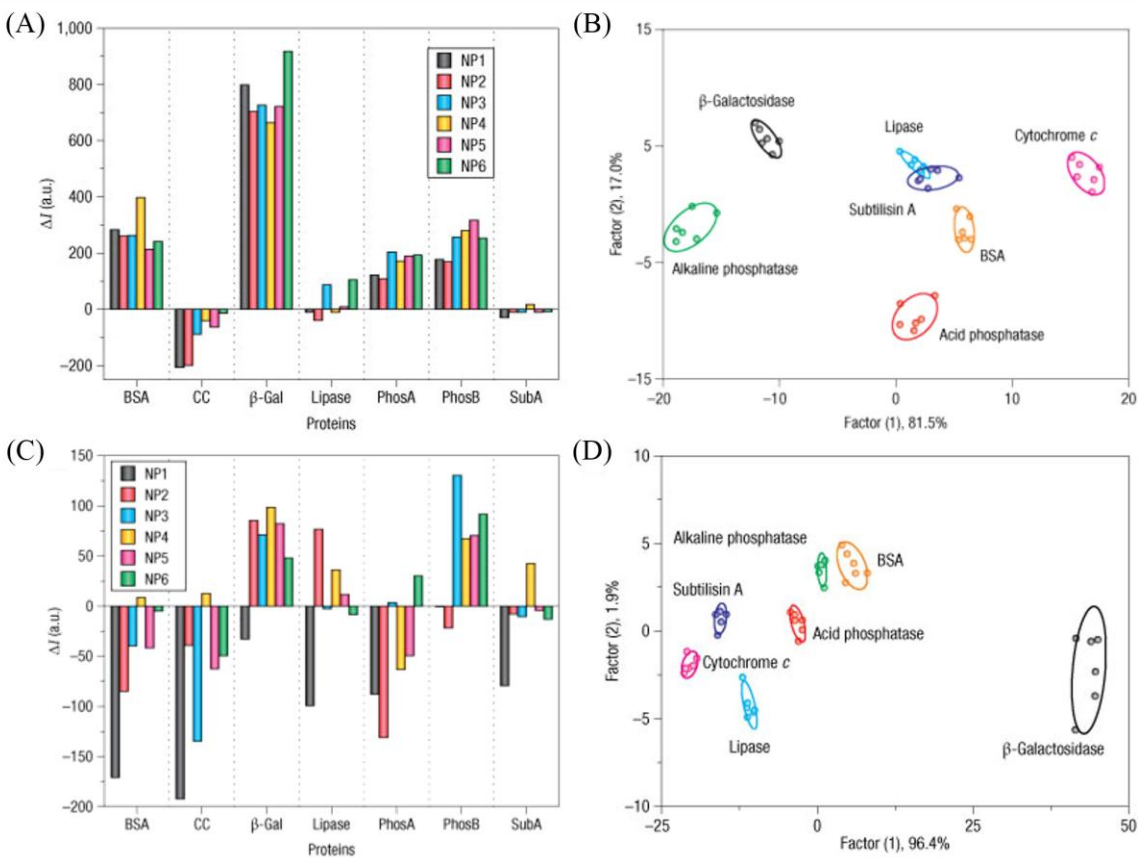

Fig. 7. Array-based sensing of protein analytes at 5 μM and 280 nm proteins. (A) Fluorescence response (Δ*I*) patterns of the NP-PPE sensor array against 5 μM various proteins. (B) Canonical score plot for the first two factors of simplified fluorescence response patterns obtained with NP-PPE assembly arrays against 5 μM proteins. The canonical score is calculated by LDA. (C) Fluorescence response (Δ*I*) patterns of the NP-PPE sensor array against 280 nm various proteins. (D) Canonical score plot for the first two factors of simplified fluorescence response patterns obtained with NP-PPE assembly arrays against 280 nm proteins.

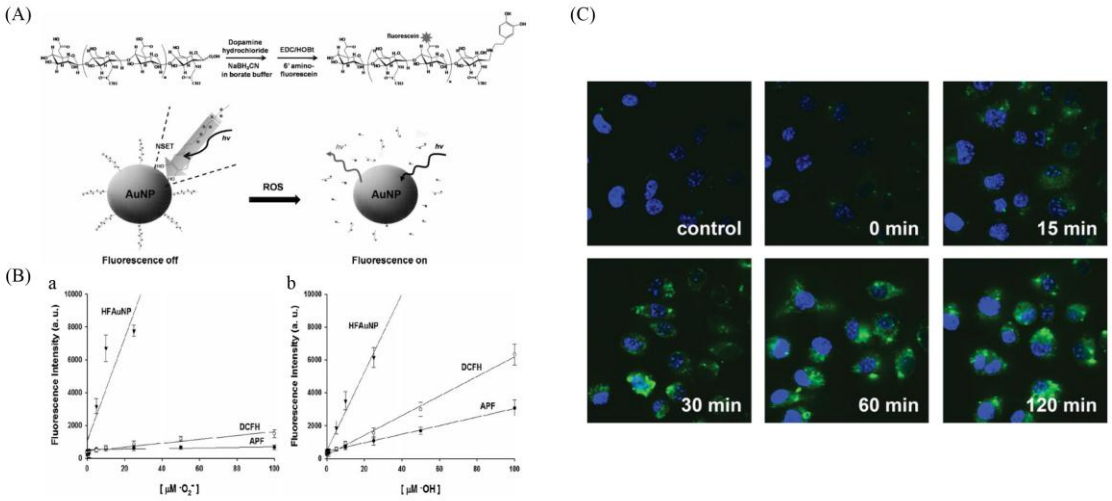

Fig. 8. (A) Schematic illustration of (a) the synthesis of dopamine end-functionalized HA and (b) the NEST–based on/off mechanism with ROS detection of gold nanoprobes with HA. (B) Graph of the ROS-detection sensitivity of HFAuNPs, showing the fluorescence intensity of the materials (HAuNPs, DCFH, APF) with (a) $^{\cdot}O_2^-$ and (b) $^{\cdot}OH$ treatment. (C) Confocal microscope analysis of intracellular ROS generation in macrophage cells. Fluorescence (green) indicates the ROS-induced cleavage of AuNP-HA conjugates and Hoechst 33628 (blue) was used for staining the nucleus of the cells.

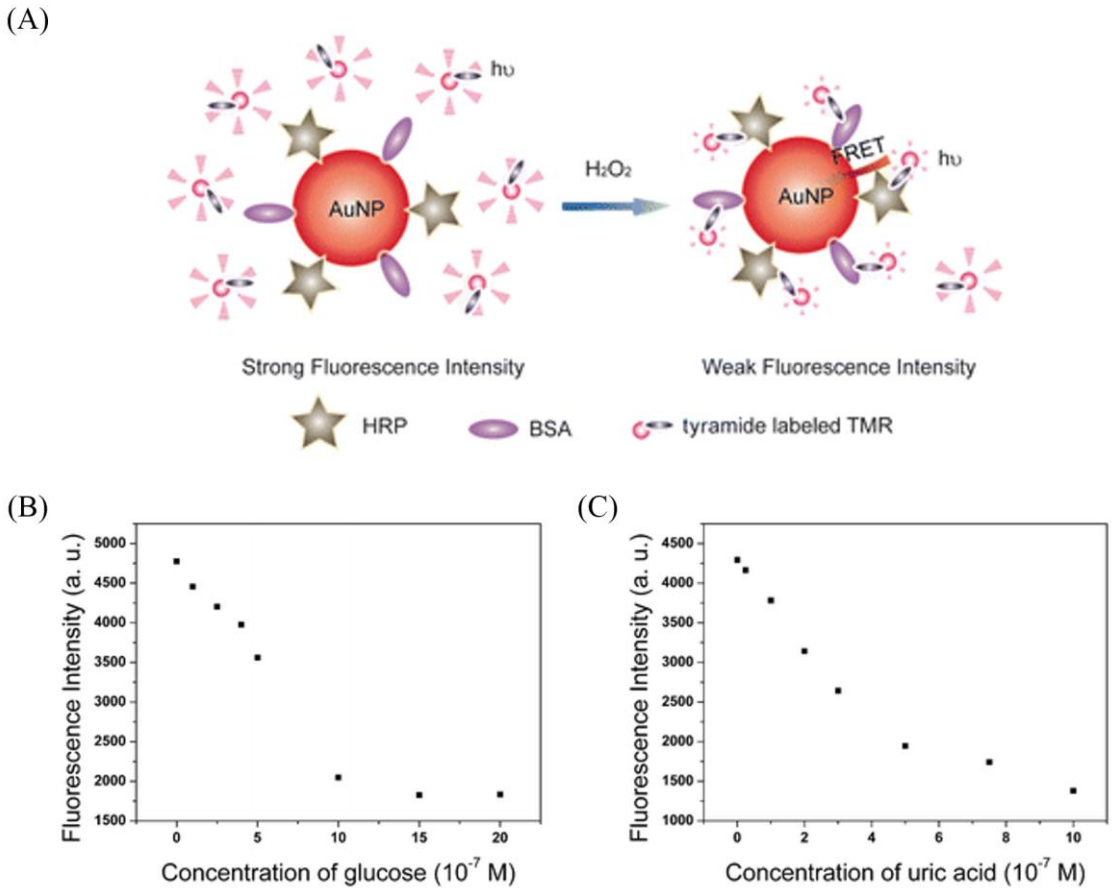

Fig. 9. (A) Schematic illustration of the FRET system between tyramide-labbeled TMR and AuNPs-HRP. (B) Graph of the relationship between the glucose concentration and the TMR fluorescence intensity (575 nm). (C) Graph of the relationship between the uric acid concentration and the TMR fluorescence intensity (575 nm).

(Reprinted with permission from (Huang et al., 2012). Copyright © 2012, Royal Society of Chemistry)

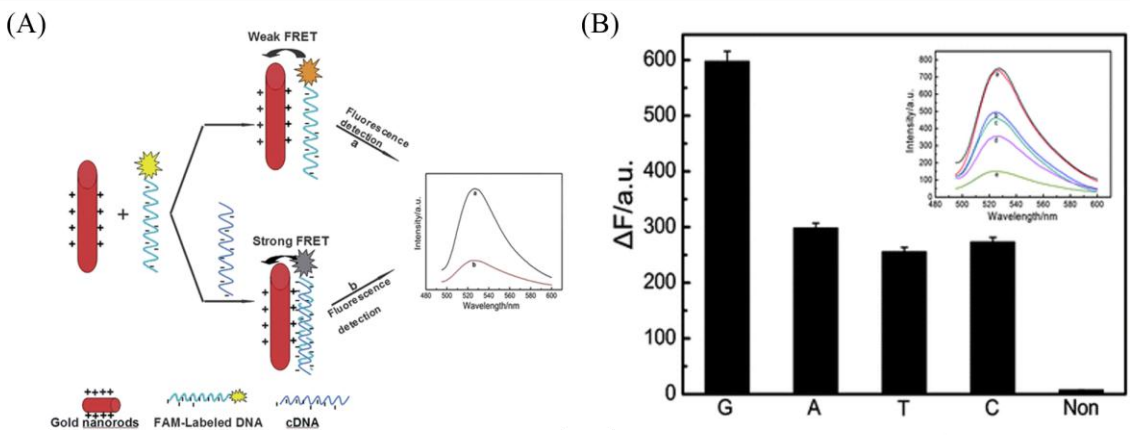

Fig. 10. (A) Schematic illustration of the strategy for DNA hybridization detection. (B) Histograms of the fluorescence intensity of probe DNA hybridization with three different DNA sequences (non-complete complementary sequences (Non); single-base mismatched sequences (A, T and C); complete complementary sequences (G)).

(Reprinted with permission from (Lu et al., 2013). Copyright © 2012, Royal Society of Chemistry)

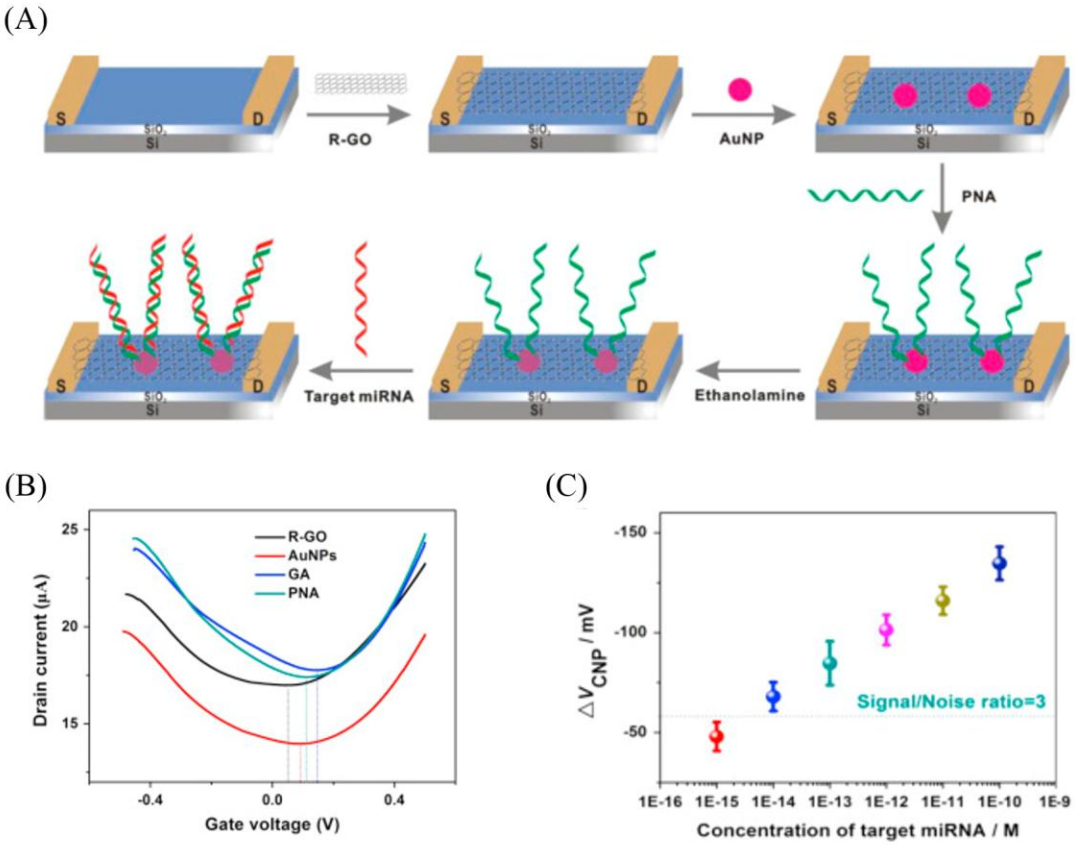

Fig. 11. (A) Schematic illustration of DNA detection and illustration of the possible molecular binding on graphene-FETs. (B) Graph showing the results of enhancement by reporter DNA-Au NP conjugates. (C) Statistics showing the results of detection target miRNA.

(Reprinted with permission from (Cai et al., 2015). Copyright © 2015, Elsevier Publishing)

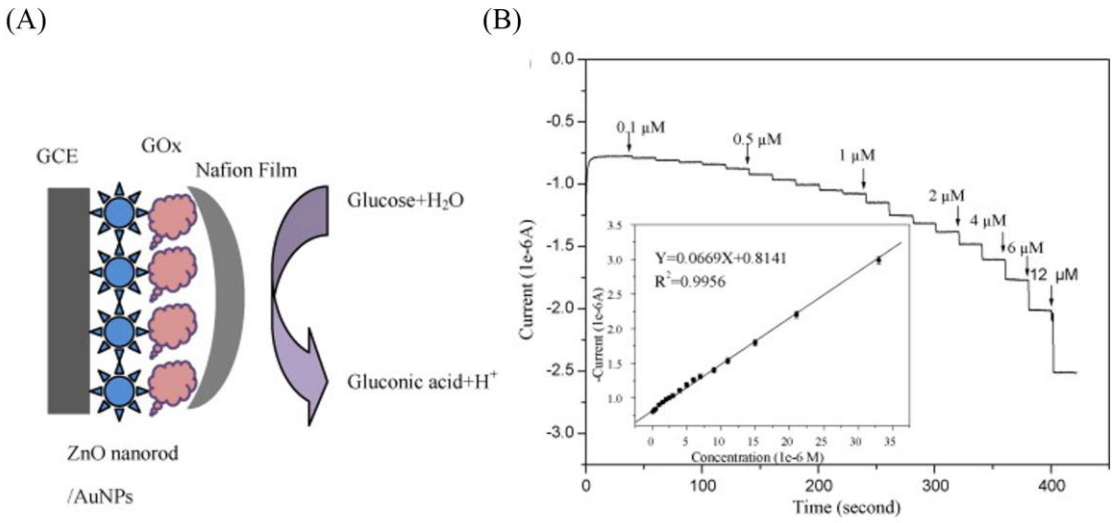

Fig. 12. (A) Structure of the glucose detection system using ZnO NRs/Au nanocomposites-modified glassy carbon electrode. (B) Change of current upon various concentrations of glucose in PBS in pH 7.4, 0.1M PBS at 0.55V (vs. Ag/AgCl).

(Reprinted with permission from (Wei et al., 2010). Copyright 2010, Elsevier Publishing)

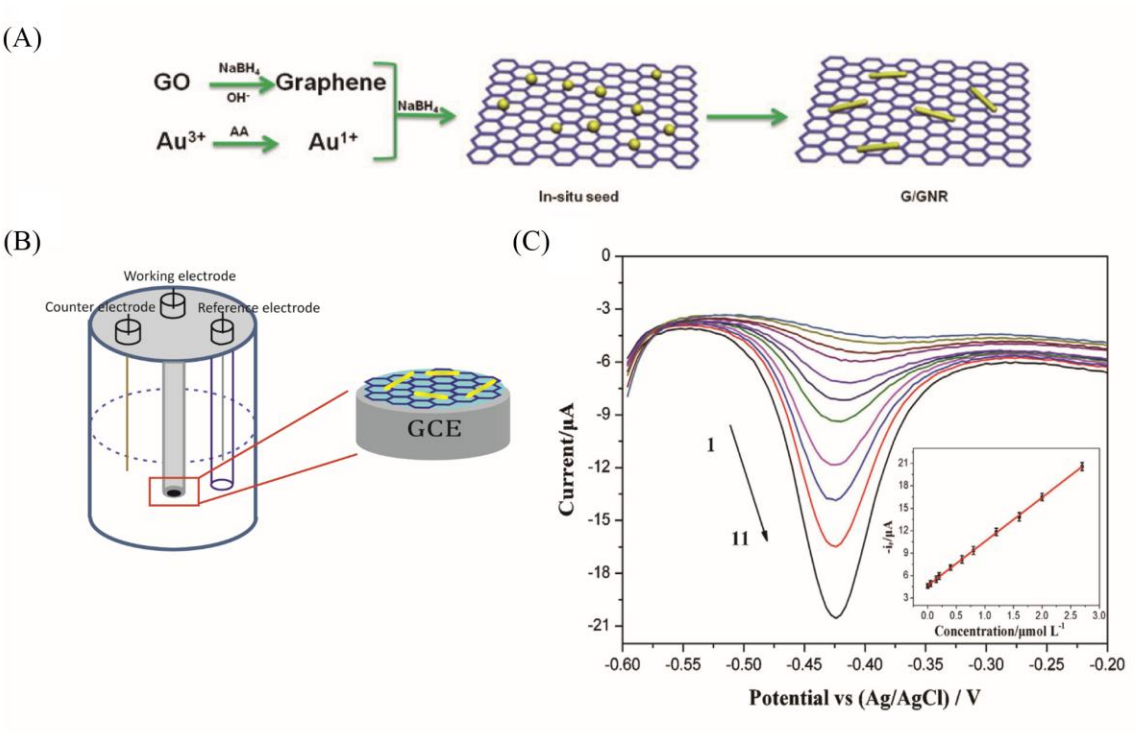

Fig. 13. (A) Diagram of the synthesis of G/AuNR composites. (B) Schematic illustration of the measuring device. (C) DPVs for different concentrations of ractopamine on G/AuNR-modified electrode after accumulation for 3 min.

(Figure (A) and (C) are reprinted with permission from (Bai et al., 2014). Copyright 2014, Elsevier Publishing)

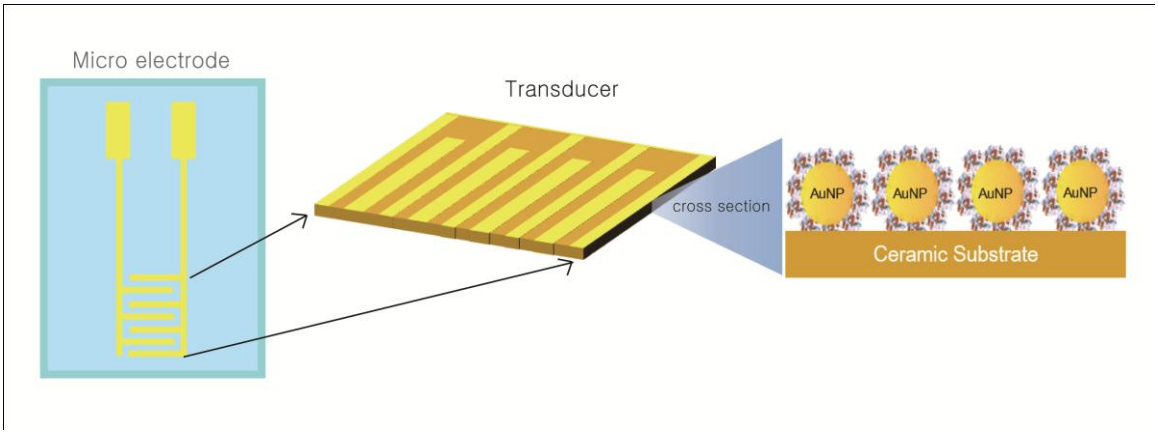

Fig. 14. Schematic illustration of the device structure of the conductometric micro electrode structures. Interdigital gold electrodes are connected with modified transducer. Nouira W. *et al* immobilized the proteinase K coated AuNP on the transducer.

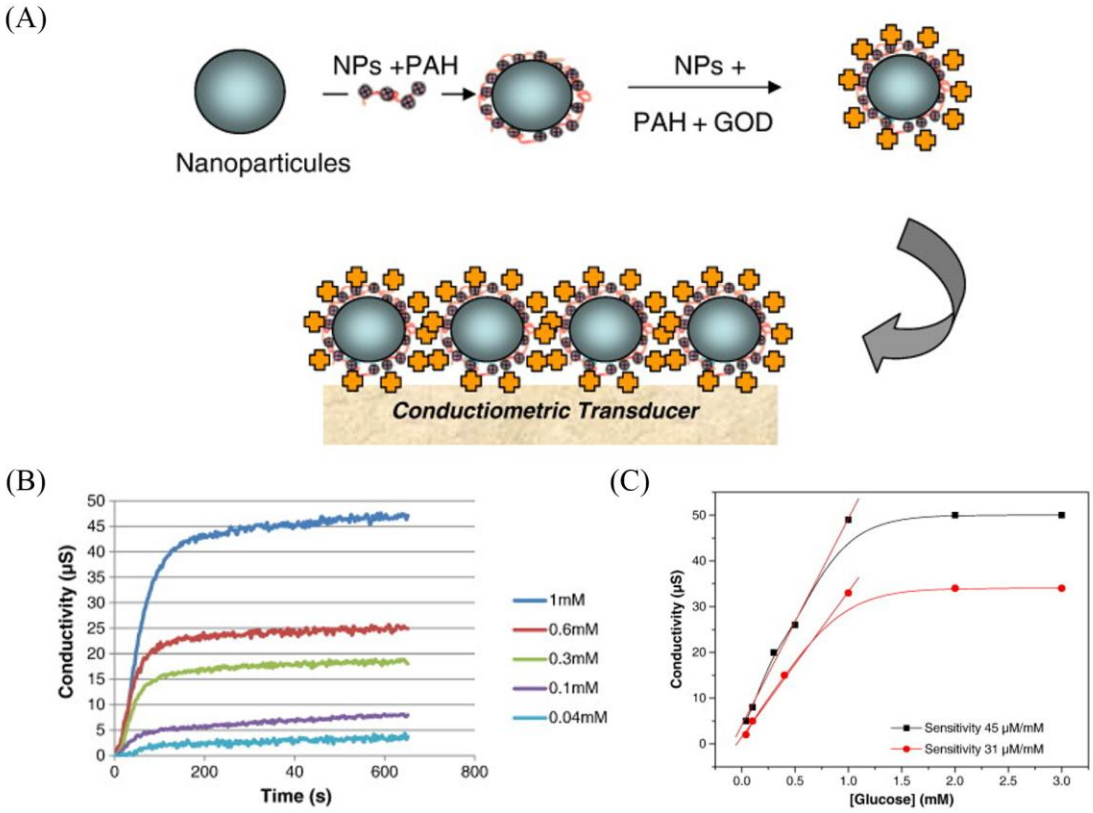

Fig. 15. (A) Schematic illustration of the device structure of modified electrode for glucose detection. (B) Graph showing the conductance response of the glucose sensor in the presence of AuNPs (5 mM phosphate buffer, pH=7.3). (C) Calibration curve of glucose sensor with and without functionalized AuNPs.

(Reprinted with permission from (Nouria et al., 2013). Copyright © 2013, Elsevier Publishing)

Highlights

- Gold-based hybrid materials offer multi-functionalities in molecular detection.
- Gold-based hybrid materials offer enhanced sensitivity and detection limit.
- Gold-based hybrid materials are categorized by three distinct detection approaches.
- Mechanism and limit of molecular detection of hybrid materials are provided.